AV

MSc Clinical Neuroscience dissertation

Evidence of disease resistance in cholinergic synapses on spinal motor neurons in a mouse model of amyotrophic lateral sclerosis

Kathleen Davis

Sobell Dept. of Motor Neuroscience, Institute of Neurology, University College London, England

July 31, 2008

ProQuest LLC
789 East Eisenhower Parkway
P.O. Box 1346
Ann Arbor, MI 48106-1346

Abstract

Transgenic mice with a mutant human Cu/Zn superoxide dismutase 1 (SOD1) gene have provided a valuable model of the human disease amyotrophic lateral sclerosis (ALS). ALS is caused by the progressive degeneration of motor neurons (MNs) in the motor cortex, brainstem and spinal cord, which involves a progressive decrease in the number of synapses contacting MNs. Previous studies have indicated that the cholinergic C-type synapse exhibits an increase in size and number on spinal MNs in the clinical stages of human ALS and animal models of ALS, which is contrary to the extensive general synaptic loss seen in the disease. This study examined the frequency and size of cholinergic, putative C-type synapses contacting ventral horn motor neurons in the lumbar spinal cord of clinically affected Tg mice carrying a $Gly^{93} \rightarrow$ Ala (G93A) mutant SOD1 gene found in familial ALS (fALS). General synaptic loss was also assessed in order to provide a base comparison with cholinergic synapse frequency. Immunocytochemical analyses were performed for synaptophysin (SP) and vesicular acetylcholine transporter (VAChT) proteins in order to measure general synapse frequency and cholinergic synapse frequency, respectively. Mice were examined at an early presymptomatic stage (aged 9-11 weeks), a transitional stage (aged 13 weeks) and a late end-stage (aged 16-20weeks). Transgenic mice exhibited a much larger progressive reduction of the immunoreactivity for SP compared to Wt mice. In contrast, immunostaining for VAChT revealed similar levels of immunoreactivity at late end-stage in both Wt and Tg mice. Measuring the widths of VAChT-immunoreactive synapses showed a significantly larger increase in synapse width in Tg mice from early stage to late stage compared to Wt mice. These results provide evidence supporting previous electron microscopy findings indicating that synapses, defined ultrastructurally as C-type, increase in frequency and size on surviving MNs at a late clinical stage in humans and

mice. The ability of putative C-synapses to resist general synaptic loss may provide a defense mechanism for spinal MNs in the present model of fALS.

ABBREVIATIONS

AChE: acetylcholinesterase

AD: autosomal dominant

ALS: amyotrophic lateral sclerosis

Bp: base-pair

ChAT: choline acetyltransferase

CNS: central nervous system

CSA: cross-sectional area

EM: electron microscopy

fALS: familial amyotrophic lateral sclerosis

G93A SOD1: SOD1 gene with an amino acid substitution of glycine at position 93 by alanine

GAP-43: growth-associated protein-43

IR: immunoreactive

M-2: muscarinic acetylcholine receptor-2

MN: motor neuron

PCR: polymerase chain reaction

rER: rough endoplasmic reticulum

SOD1: Cu/Zn superoxide dismutase 1

SP: synaptophysin

SSC: sub-synaptic cistern

Tg: transgenic

VAChT: vesicular acetylcholine transporter

VAMP-2: vesicle-associated protein 2

Wt: wild-type

Acknowledgments

I would like to thank Dr. Anthony Pullen for supervising my research project and generously volunteering his time and assistance throughout the development of my thesis.

I am also grateful to Dimitra Athanasiou, research assistant to Dr. Pullen, for demonstrating lab techniques and providing advice and encouragement.

Statement of contributions

The study design was provided by Dr. Pullen and modified throughout the course of the project based on mutual discussion. I was able to participate and assist in all aspects of the study methods at least once, excluding handling of live animals, which was done exclusively by Dr. Pullen under approved British Home Office license. After receiving training from Dr. Pullen and Dimitra Athanasiou, I independently carried out tissue sectioning, immunocytochemistry techniques and data analysis. Statistics were carried out independently after consulting with Dr. Pullen and Dr. Constantinos Kallis.

CONTENTS

1. Introduction

1.1. Amyotrophic lateral sclerosis/motor neuron disease characteristics

Amyotrophic lateral sclerosis (ALS), also referred to as motor neuron disease, was first recognized by Jean-Martin Charcot in 1869 as a syndrome consisting of progressive muscular atrophy often involving bulbar muscles but not affecting the nuclei controlling eye movements or Onuf's nucleus controlling bladder and bowel function (Swash & Schwartz, 1995; Al-Chalabi, 2006). ALS is caused by progressive motor neuron (MN) degeneration in the motor cortex, brainstem and spinal cord (Swash & Schwartz, 1995). Classical ALS involves degeneration of upper MNs found in the cortex, as well as lower MNs found in the brainstem and spinal cord. Degeneration of axons of upper MNs disrupts direct and indirect signaling to lower MNs in the spinal cord and leads to the characteristic feature of primary lateral sclerosis of the corticospinal tract (Boillee et al., 2006). Lower MN loss disrupts signaling from brainstem MNs to facial, neck and eye muscles, as well as signaling from spinal cord MNs to all other voluntary muscles of the body, which leads to the progressive and eventually fatal paralysis seen in ALS (Boillee et al., 2006).

Spinal MN loss is particularly prominent in the ventral horn and is paralleled by a loss of large myelinated fibers in the ventral roots and peripheral motor nerves (Tandan & Bradley, 1985a). ALS patients also exhibit significant loss of spinal interneurons, found primarily in the dorsomedial quadrant (Stephens et al., 2006). In addition, the motor cortex of ALS patients was found to contain significantly more phosphorylated neurofilaments and markers of astrocytosis compared to age-matched non-neurological controls (Sasaki & Iwata, 1999).

The disease typically presents in mid to late life (Wong et al., 1995) and hallmark characteristics of the disease include muscle weakness and wasting, fasciculation, spasticity, hyperreflexia, and Babinski reflex. Frequently there are bulbar symptoms such as dysphagia

and dysarthria (Swash & Schwartz, 1995). Disease onset in adults typically presents as asymmetric weakness of two or more limbs and then progresses to complete paralysis with death typically occurring within a few years of symptom onset due to respiratory failure (Mulder, 1982; Al-Chalabi, 2006). Only one in five people with ALS survives five years, while only one in ten survives 10 yrs or more (Al-Chalabi, 2006). Annual incidence of the disease is approximately 1-2 per 100,000 people worldwide (Tysnes, 2004) and the prevalence is approximately five in 100,000 people (Al-Chalabi, 2006). Men are 1.5 times more likely to be diagnosed with ALS than women and studies have proposed increased risk in population groups including professional Italian footballers and Gulf War veterans (Horner et al., 2003; Chio et al., 2005; Al-Chalabi, 2006).

Approximately 10% of ALS cases are familial and most of these are autosomal dominant (AD) (Mulder et al., 1986; Siddique et al., 1989). Of those patients with AD familial ALS (fALS), 15-20% have missense point mutations in the gene encoding cytosolic Cu/Zn superoxide dismutase 1 (SOD1), a well-known antioxidant enzyme (Deng et al., 1993; Rosen et al., 1993). The genes alsin, VAP13 and senataxin have also been identified as causes of fALS and several genes found in large population genetic studies are thought to be risk modifiers for sporadic forms of ALS (Yang et al., 2001; Chen et al., 2004; Kunst, 2004; Nishimura et al., 2004). Symptoms & pathology of fALS are mirrored in sporadic ALS patients (Morrison et al., 1998b), indicating that the two forms of disease have similar pathological processes.

1.2. Animal models of ALS

While post mortem studies of ALS are useful in studying the end-stage pathology of the disease, animal models are necessary to examine pre-clinical and intermediate stages of the disease. Transgenic (Tg) mice expressing mutant forms of SOD1 that are found in fALS

patients are used to model fALS caused by SOD1 mutations. There are four mouse models that mimic clinical features and end-stage pathology seen in fALS and the SOD1 mutations that account for these models include G93A, G37R, G85R and G86R.

Primary pathology of the SOD1 mouse is characterized by progressive MN loss in the lumbar spinal cord and brainstem and the main clinical sign is progressive muscle weakness and atrophy leading up to end-stage paralysis (Gurney, 1997; Zang & Cheema, 2002). Mice expressing high levels of mutant SOD1 exhibit earlier symptom onset than those expressing low levels of mutant SOD1 (Wong et al., 1995; Bruijn et al., 1997a; Dal Canto & Gurney, 1997). Age of onset varies from 100-225 days depending on level of expression and mutation type, but all Tg mice display rapid progression from onset of muscle weakness to total paralysis (~2 weeks) (Morrison et al., 1998b; Elliott, 1999). Onset of MN loss generally coincides with onset of muscle weakness and MN loss at end stage is ~ 50% in studies that quantified neuronal loss (Chiu et al., 1995; Wong et al., 1995; Morrison et al., 1996; Bruijn et al., 1997a; Morrison et al., 1998a). Other common pathological characteristics seen among Tg mice include astrocytosis, cytoskeletal abnormalities, cytoplasmic ubiquitination, axonal swellings due to neurofilament accumulation and Lewy-like bodies (Gurney, 1997). For clinical features, disease time-course and pathology of individual Tg animal models see Table 1.

MN loss in SOD1 mice appears to be selective for large MNs according to a study by Mohajeri et al. (1998), which examined MNs innervating the medial gastrocnemius muscle of G93A SOD1 mice. This study found that MNs with a diameter greater than 20μm declined to 36% of that in normal mice by 18 weeks, while MNs with a diameter less than 20μm remained relatively unchanged. G93A SOD1 mice also exhibit a distal-to-proximal degeneration of MNs and ventral root motor axons (Fischer et al., 2004).

1.3. Commonalities of disease in human ALS and mouse models

Transgenic animal models of ALS are an effective means for studying the clinical and pathological development of the disease as several primary disease features are found in both SOD1 mice and familial ALS. Progressive weakness and muscle atrophy leading up to complete paralysis is the primary clinical feature shared in human ALS and mouse models of the disease. Motor neuron and interneuron loss, as well as phosphorylated neurofilament inclusions and reactive astrocytosis, are found in both SOD1 mice and familial ALS (Oyanagi et al., 1983; Chiu et al., 1995; Wong et al., 1995; Bruijn et al., 1997a; Tu et al., 1996; Morrison et al., 1996, 1998; Kong & Xu, 1998). Also common to mice and humans are vacuoles and SOD1 inclusions (Dal Canto & Gurney, 1995; Wong et al., 1995; Mourelatos et al., 1996; Bruijn, 1997a). Autonomic MNs were found spared in G93A mice (Chiu et al., 1995) and MNs in the spinal nucleus of the bulbocavernosus, which is the rat and mouse homologue of human Onuf's nucleus in the sacral spinal cord, are relatively spared in slow and fast progressing mice (Hamson et al., 2002). Autonomic MNs and MNs in Onuf's nucleus are frequently spared in ALS patients (Kiernan & Hudson, 1993; Pullen & Martin, 1995). Significant degeneration of corticospinal and bulbospinal projections are seen in G93A SOD1 mice by retrograde labeling, with corticospinal projections representing the hindlimbs and located mostly in the medial sensorimotor cortex. This pattern resembles late stages of human ALS, which involve loss of descending motor control by descending cortical and bulbar neurons (Zang & Cheema, 2002).

1.4. Mutant SOD1 & mechanisms of MN death

Superoxide dismutase protein is found in almost all cells of the body and is present in the cytoplasm of both neuronal and non-neuronal cells in the central nervous system (CNS) (Pardo et al., 1995).

Mutation: G93A SOD1 (human)
Onset: 90-190 days (Chiu et al., 1995; Feeney et al., 2001) ▪ tremor followed by limb weakness & impaired extension of hindlimb (Gurney et al., 1994; Chiu et al., 1995; Morrison et al., 1998b; Feeney et al., 2001) ▪ Neuro-muscular changes begin @ 63-90 days (Azzouz et al., 1997)
End-Stage: 130-140 days (Azzouz et al., 1997), 273 days (Feeney et al., 2001) ▪ 27% weight reduction (Azzouz et al., 1997)
Key Clinical Features ▪ Tremor, spasticity, hyperreflexia, crossed spread of spinal reflexes, muscle weakness & atrophy usually more evident in hindlimbs (Chiu et al., 1995)
General Pathology ▪ Vacuoles in spinal and cranial MNs & related areas of brainstem due to swollen mitochondria (Chiu et al., 1995) ▪ Severe loss of large myelinated axons from ventral motor roots & peripheral nerves (Gurney et al., 1994; Chiu, 1995) ▪ Ubiquitin+ axonal processes in ventral horn (Feeney et al., 2001) ▪ phosphorylated neurofilament neuronal inclusions (Gurney et al., 1994) ▪ Swollen axons with dense axoplasm (Gurney et al., 1994). ▪ Autonomic MNs spared and denervation and reinnervation of skeletal muscle occured along with MN loss (Chiu et al., 1995) ▪ relative sparing of brainstem motor neurons innervating the face (Azzouz et al., 1997) ▪ 26% reduction in dopaminergic neurons of SN (Kostic et al., 1997)

Mutation: G37R SOD1 (human)
Onset: 105-180 days (Morrison & Morrison, 1999); 352 days in late-onset Tg models (Urushitani et al., 2007)
End-Stage: 330-385 days in late-onset Tg models (Nguyen et al., 2003; Urushitani et al., 2007), end-stage not found for younger-onset mice
Key Clinical Features ▪ Tremor followed by limb weakness (Morrison et al., 1998b)
General Pathology ▪ Mitochondrial degeneration with swelling and altered cristae in spinal and brainstem MNs (Wong et al., 1995) ▪ MN loss & neurofilament protein inclusion at symptom onset; reactive astrocytosis and vacuoles prior to symptom onset (Morrison & Morrison, 1999)

Mutation: G85R SOD1
Onset: 240-300 days (Bruijn et al., 1997a)
End-Stage: 254-314 days (Bruijn et al., 1997a)
Key Clinical Features ▪ Hindlimb weakness & atrophy (Bruijn et al., 1997a; Morrison et al., 1998b)
General Pathology ▪ Astrocytic SOD1-containing inclusions in spinal cord prior to symptom onset; significantly increased astrocytosis by end-stage (Bruijn et al., 1997a)

Mutation: G86R SOD1
Onset: 90-105 (Ripps et al., 1995)
End-Stage: 110-120 days (Ripps et al., 1995)
Key Clinical Features ▪ Limb weakness, spastic paralysis, muscle wasting (Ripps et al., 1995; Morrison et al., 1998a)
General Pathology ▪ Loss of MNs in spinal cord, brain stem and cortex (Ripps et al., 1995) ▪ Loss of spinal interneurons (Morrison et al., 1998a) ▪ Accumulated phosphorylated NF inclusions (Morrison et al., 1998a) ▪ Reactive astrocytosis (Morrison et al., 1998a) ▪ Dystrophic neurites in VH gray matter, swollen & fragmented neuronal processes (Ripps et al., 1995)

Table 1. Clinical and pathological characteristics of the four SOD1 Tg mouse models of ALS.

SOD isoforms function as free radical scavengers (Wong et al., 1995) and are involved in regulating the cell's response to oxidative stress and preventing damage caused by oxygen radicals (Halliwell, 1994; Yu, 1994). SOD is able to convert superoxide radicals (O_2^-) to hydrogen peroxide and this reaction [$2O_2^- + 2H^+ \rightarrow H_2O_2 + O_2$] is catalyzed by Cu^{+2} in the protein's active site. This process prevents the oxidation of proteins and the peroxidation of lipids (Halliwell et al., 1992; Olanow & Arendash, 1994). It is purported that both increases and decreases in the level of normally functioning SOD protein have the potential to enhance oxidative stress (Shibata, 2001).

It was at one time proposed that the neurodegenerative nature of ALS was caused by a reduction in SOD1 superoxide radical clearance activity due to loss of function mutations but this is unlikely due to the autosomal dominant transmission of mutant SOD1 familial ALS and its Tg mouse model. It was shown separately by Borchelt et al. (1994) and Fujii et al. (1995) that some mutant forms of SOD1 maintain the ability to clear away superoxide radicals but still cause the neurodegenerative ALS phenotype in patients and Tg mice. Further refuting the loss-of-function theory is the finding that clinical severity of ALS patients is not correlated with SOD1 enzyme activity levels (Shibata, 2001). In addition, SOD1 knockout mice, as well as wild-type (Wt) SOD1-overexpressing mice do not develop ALS symptoms (Reaume et al., 1996; Shibata, 2001).

Since these findings, several disease mechanisms have been proposed, which involve a toxic gain-of-function of SOD1. These include oxidative injury, peroxynitrite toxicity, neurofilament accumulation, glutamate excitotoxicity, excessive Ca^{2+} influx, apoptosis, SOD1 aggregation and carbonyl stress. Oxidative injury was originally proposed to be a result of SOD1 mutations, however, several studies contradict this theory and recent in vitro evidence shows that there is no difference in the oxidative stress levels generated by mutant and Wt SOD1 enzymes (Bruijn et al., 1997b; Jaarsma et al., 1998; Shibata et al., 2000a;

Shibata et al., 2000b). Peroxynitrite toxicity was suggested as a disease mechanism in a study showing that mutant SOD1 catalyzes the nitration of tyrosine residues by peroxynitrite more readily than the dismutation of superoxide (Ischiropoulos & Al-Mehdi, 1995). Neurofilament light subunits of the cytoskeleton were found to accumulate, often in their phosphorylated form, in MNs and swollen axons in ALS patients and SOD1 Tg mice, suggesting that impaired axonal transport may play a role in disease pathology (Kusaka & Hirano, 1999; Shibata et al., 2000b). Indeed, studies of Tg mouse models of ALS have demonstrated impairment in both slow and fast axonal transport, which appears before significant loss of spinal motor neurons and peripheral axons (Warita et al., 1999; Williamson & Cleveland, 1999).

Bruijn and colleagues (1997a) proposed that reductions of glial glutamate transporter (GLT-1), a major glutamate transporter in the spinal cord, points to glutamate toxicity as a mechanism for MN degeneration. In contrast, a study by Schutz (2005) found reductions in vesicular glutamate transporter-1 and -2 appositions to MN soma paralleled by unchanged vesicular inhibitory amino acid transporter appositions, implicating over-inhibition as a pathological mechanism rather than over-excitation. Another theory is that SOD1 mutations alter glutamate transporters or receptors in such a way that leads to activation of non-NMDA glutamate receptors and increased intracellular calcium (Morrison & Morrison, 1999). Altered ionic homeostasis could then lead to mitochondrial dysfunction, accumulation of neurofilament and activation of cellular enzymes with all of these effects leading to cell death. Aggregation of SOD1, which is seen in lower MNs of SOD1 mutant fALS patients and Tg mice, is suspected of playing a role in ALS pathology but its exact role in neurodegeneration is unclear. As in other neurodegenerative diseases involving abnormal protein aggregation, SOD1 aggregates may disrupt protein quality-control mechanisms such as chaperones, autophagy and the ubiquitin-proteasome system. SOD1 inclusions are also

implicated in the enhancement of protein carbonylation, which may have neurotoxic effects (Shibata et al., 2000b). Studies of Tg mice have indicated that several neurotoxic processes overlap (Morrison et al., 1998b), but the overarching mechanism of MN death, and how to prevent it, is still unknown.

1.5. Axonal sprouting and neuromuscular interactions in ALS

In addition to studying mechanisms of neurodegeneration, research in ALS is also focused on neuromuscular interactions and synaptic alteration. As a result of muscle denervation in mutant SOD1 mice, MNs send collateral axon sprouts to denervated skeletal muscle fibers during the same period in which MN loss occurs (Chiu et al., 1995). GAP-43, a neuronal growth-associated protein found enhanced in growth cones and nerve synapses, is thought to be involved in axonal growth and synaptogenesis (Neve et al., 1987; Skene, 1989) and may contribute to muscle reinnervation in ALS by facilitating axonal sprouting. Using Northern blot analysis and in situ hybridization, Parhad et al. (1992) demonstrated a 2- to 4-fold increase in (GAP)-43 gene expression in the ventral horn cells of ALS patients compared to controls. Immunocytochemistry also identified a dense accumulation of GAP43 immunoreactivity in ventral horn cells and their neuronal processes in ALS patients (Ikemoto et al., 1999). Another study, which examined muscles from 8 patients with ALS, found GAP-43 expressed only in severely atrophic muscle fibers (Ueki et al., 1993), although it remains unclear whether this indicates a protective function.

Although GAP-43 is expressed in regenerated nerve synapses (Verhaagen et al., 1988; Skene, 1989), findings of extensive collateral sprouting in ALS (Wohlfart, 1957) but little regeneration (Tandan & Bradley, 1985b) suggests that GAP-43 gene expression in ALS is correlated with collateral sprouting rather than regeneration after axonal injury. These findings may reflect an enhanced response of surviving motor neurons to overcome disease

by sending collateral axons to denervated muscle fibers. However, other groups have postulated that accumulation of GAP43 on ventral horn cells is due to an abundance of GAP-43 in afferent synapses attached to the ventral horn cells (Ikemoto et al., 1999). This may indicate a compensatory mechanism involving afferent nerves sprouting out to ventral horn cells, in response to surrounding degeneration, and carrying an abundance of GAP-43 due to their regenerative nature. This theory is supported by evidence that in the spinal cord of rats with peripheral nerve injury, GAP43 accumulation on ventral horn cells seems to be associated with reorganization of afferent synapses (Knyihar-Csillik et al., 1992). Whether an indication of afferent sprouting or MN axonal sprouting, high levels of GAP43 in ventral horn cells suggest that cells in this area have a specialized ability to retain through adulthood the potential for functional and structural changes or ongoing synaptic remodeling.

Electrophysiological recordings of the neuromuscular unit in the medial gastrocnemius muscle of G93A Tg mice revealed that by 100 days the compound muscle action potential amplitude decreased by 24% but the number of motor units was reduced by 53% (Azzouz et al, 1997). The same study found that the motor unit potential in Tg mice to be similar to controls, suggesting that surviving motor units remain functionally intact. These findings support the theory that MNs sprout collateral axons to compensate for the loss of motor units and imply that as motor units decrease in number they increase in size. Neuromuscular functional impairment was shown to occur prior to the onset of MN loss in G93A SOD1 mice (Kennel et al., 1996), lessening the likelihood that MN loss is a direct cause of neuromuscular dysfunction in ALS. It is possible that neuromuscular dysfunction causes MN death in a retrograde manner, but it is also likely that events leading up to MN loss, such as mitochondrial damage and axonal transport dysfunction, result in failure at the neuromuscular junction.

1.6. Synaptic alterations among spinal MNs in ALS

Alterations in synaptic synapses are a prominent feature of ALS pathology. Distinct ultrastructural changes such as accumulation of dark presynaptic vesicles and dark mitochondria with dense cristae occur in presynaptic synapses contacting the large cortical Betz cells in ALS patients (Sasaki & Iwata, 1999). General synaptic loss is also a prominent characteristic in ALS pathology and is often measured by examining the reduction of synaptophysin (SP), a major membrane protein of small synaptic vesicles in presynaptic synapses throughout the nervous system (Navone et al., 1986). Ikemoto and Hirano (1996) compared SP immunostaining in 4 sporadic ALS patients to that seen in 6 non-neurological controls. SP immunoreactivity in sporadic ALS patients was diffusely decreased in the ventral horn of the lumbar cord with more extensive reductions in the lateral portion of the ventral horns, whereas immunoreactivity in other gray matter areas of the spinal cord was preserved. Light microscopical examination of SP immunostaining on synaptic synapses in G93A SOD1 Tg mice confirms a significant reduction in SP-immunoreactive (SP-IR) synapse density on CNS MN soma and proximal dendrites (Zang et al., 2005).

Synaptic alterations in ALS are also caused by axonal sprouting, which appears to occur as surviving MNs attempt to re-establish communication with other nerve cells or muscle fibres by sprouting collateral axons. Under normal conditions, spinal MNs may be contacted by a variety of presynaptic synapses that are classified ultrastructurally into five types including S-, F-, C-, M- and T-type (Bodian, 1966; Conradi, 1969a,b; McLaughlin, 1972; Boone & Aldes, 1984). The relatively large C-type synapse (3-5μm) is found contacting large α-MNs in the brainstem and spinal cord and is defined by densely packed synaptic vesicles and a membranous cistern beneath the postsynaptic membrane subtended by layers of rough endoplasmic reticulum (rER) interspersed with ribosomes (Pullen &

Sears, 1978; Hellstrom et al., 1999). There is evidence that the distinctive C-synapse may undergo alterations as part of a compensatory measure after spinal cord injury or in ALS. The C-synapse was found to increase in size and numbers on thoracic MN somata and proximal dendrites in the ventral horn of cats after partial central deafferentation (Pullen & Sears, 1978). After deafferentation, the increase in synaptic size involved a lengthening of sub-cisternal layers of rER. The increased number of C-synapses involved the appearance of these synapses and sub-cisternal stacks of rER on dendrites not normally exhibiting C-synapses (Pullen & Sears, 1978).

Alterations in C-synapses have also been observed in ALS patients and G93A SOD1 Tg mice. Electron microscopy (EM) studies of spinal MNs of patients who died from ALS suggested a selective resistance and enlargement of the C-synapse (Pullen et al., 1992). Subsequent EM follow-up studies with Tg mice carrying the mutated human SOD1 gene indicated that C-synapses progressively increase in size and number on surviving spinal MNs. The increase in size of C-synapses is accompanied by progressive lengthening of sub-synaptic rER layers as well as an increase in the number of rER lamellae (Pullen & Athanasiou, 2007). These findings could be related to experiments using the G93A SOD1 mouse model of ALS, which revealed a subpopulation of disease-resistant motor units that were abnormally large and contained few degenerating synapses (Schaefer et al., 2005).

1.7. Cholinergic nature of C-synapses

Lesion evidence suggests that the origin of C-synapses is in close proximity to MNs in the spinal cord (McLaughlin, 1972) and a likely candidate are the medium to large multipolar cells in the intermediate gray matter between the dorsal and ventral horns (partition neurons), which are immunoreactive for choline acetyltransferase (ChAT) (Hellstrom et al., 1999; Miles et al., 2007). Connaughton et al. (1986) confirmed the cholinergic nature of C-

synapses in a study examining MNs in the hypoglossal nucleus of rats using light and electron microscopy. The study found that the majority of ChAT-IR synapses making synaptic contact with MN somata and proximal dendrites were C-type and contained sub-synaptic cisterns (SSCs).

Further evidence pointing to the cholinergic nature of C-synapses arises from a study of rat spinal cord, which used antibody directed against the gap junction protein connexin-32 to immunolabel SSCs in combination with ChAT and acetylcholinesterase (AChE) immunolabeling to determine whether C-synapses on MNs contained these cholinergic markers (Nagy et al., 1993). ChAT-IR and AChE-IR synapses frequently apposed immunolabeled SSCs and at the light microscope level most if not all C-synapses appeared cholinergic. Augmenting these results, Li et al. (1995) examined the facial nucleus and lumbar segment of spinal cord in adult rats using electron microscopy and found that SSCs were always subjacent to ChAT-positive synapses on both somata and large dendrites and almost always apposing AChE labeled synapses. Putative C-synapses have also been immunolabeled by vesicular acetylcholine transporter (VAChT), which is uniquely expressed in cholinergic synapses (Gilmor et al., 1996; Ichikawa et al., 1997; Schafer et al., 1998). Synthesized in the endoplasmic reticulum and Golgi apparatus, VAChT is a proton-dependent transporter that concentrates in synaptic vesicles of axon synapses and packages acetylcholine into synaptic vesicles (Gilmor et al., 1996). VAChT expression within recognized C-synapses was found to be associated with ChAT and vesicle-associated protein 2 (VAMP-2) (Gilmor et al., 1996; Hellstrom et al., 1999), as well as muscarinic acetylcholine receptor-2 (M-2), which was localized on the postsynaptic membrane of various types of MNs apposed by C-synapses (Hellstrom et al., 2003). Recordings from spinal cords of mutant SOD1 Tg mice showed that application of muscarine has the ability to activate M-2 receptors, which increases the excitability of MNs by reducing the action potential after-

hyperpolarization. In addition, endogenous cholinergic inputs increase MN excitability during drug-induced locomotion (Miles et al., 2007).

1.8. Aims of study

The aim of this study was to determine the time-course and extent of cholinergic VAChT expression in synapses contacting ventral horn MNs during disease progression in mice with ALS and to verify whether these findings are compatible with results from previous EM studies of C-synapses in experimental ALS. Immunocytochemical methods were employed in order to stain for VAChT protein in spinal cord sections taken from Tg mice carrying a G93A SOD1 gene. Immunostaining was also carried out for SP in order to determine the extent of general synaptic loss. Initially, the aims included immunostaining for VAMP-2 and M-2 in order to study the efficacy of these proteins as C-synapse markers in comparison to VAChT. However, due to the capricious nature of these antibodies and the amount of time necessary to optimize immunostaining, the present study focused on results obtained from VAChT and SP staining. The time-course and extent of VAChT expression was investigated by analyzing at an early presymptomatic stage (mice aged 9-11 weeks), a transitional stage (13 weeks) and a late end-stage (16-20 weeks).

2. Materials and Methods

2.1. Animal Model

Transgenic mice used in this study carried a mutant human SOD1 gene with an amino acid substitution of glycine at position 93 by alanine (G93A). Male mice, designated B6SJL-TgN (SOD1-G93A) 1Gur, were acquired from Jackson Laboratories (USA) and bred with B6SJL/F1 females to give mixed litters of hemizygous Tg and non-Tg Wt littermates. At around 16-20 weeks of age, the Tg mice developed progressive spasticity

and muscle weakness in one or more limbs beginning with the hindlimbs and were sacrificed when movement became severely impaired (All procedures conducted on living animals were performed by my project supervisor Tony Pullen under British Home Office approved license). The mice were divided into six groups: 9-11 week Tg (pre-clinical, n=4), 13 week Tg (transitional, n=3), 16-20 week Tg (clinically affected, n=5), 9-11 week Wt (n=6), 13 week Wt (n=3) and 16-20 week Wt (n=5). The identification and physical characteristics recorded for each mouse are listed in Appendix A.

2.2. Genotyping mutant SOD1 mice

The entire genotyping procedure involved extraction of DNA from tail biopsies, purification of DNA, amplification of DNA by polymerase chain reaction (PCR) and analysis of base-pair (bp) composition with electrophoresis. All glassware, centrifuge tubes, PCR tubes and pipette tips used were PCR grade (free of DNAase/RNAase) and autoclaved at a minimum of 121°C for 20 minutes.

DNA EXTRACTION & PURIFICATION

Complete DNA extraction and purification occurs over two days. Frozen samples of tail biopsies (0.5cm lengths cut from tips of tails from mice under local anesthetic, according to veterinary and Home Office approved license) were thawed. Samples were stored on ice until use. Tail digestion medium was prepared in an autoclaved, sterile Eppendorf tube according to the number of tails to be analyzed. For each tail, 120µl of 0.5M EDTA (pH8.0) was added to 500µl Nuclear Lysis Solution (Promega Cat No A7941) and this was vortexed for 20 seconds and then chilled on ice. Each tail biopsy was added to a fresh, autoclaved 1.5ml Eppendorf centrifuge tube and 600µl of digestion medium and 17.5µl of a 20mg/ml Proteinase-K (stored in freezer) was added to each tube. These were then vortexed for 10-20 seconds. Tubes were placed in a plastic rack, which was placed in a water bath pre-heated to

55°C (Grant, Model). Samples were incubated overnight at 55°C, with occasional gentle shaking to ensure the tissue was completely digested.

Upon digestion, tubes were removed from the water bath and samples were allowed to come to room temperature. 200µl protein precipitation solution (Promega A7951, 25ml stock) was added to each tube and then vortexed vigorously at high speed for about 20 seconds. Samples were then chilled on ice for 5 minutes, which caused a white precipitate to form. Tubes were transferred to a refrigerated centrifuge (Eppendorf Model 5402) and centrifuged for 6-10 minutes at 14,000g at 4°C, which caused precipitate to form a tight pellet. Tubes were transferred from centrifuge to the rack and supernatant was removed with a micropipette and transferred into clean autoclaved 1.5ml Eppendorf centrifuge tubes. To each tube, 600µl isopropanol (Fluka) was added and this solution was maintained at room temperature. The solution was gently mixed by inversion until white thread-like strands of DNA formed a visible mass. Tubes of DNA were centrifuged for 6 minutes at 14,000g at room temperature to form a small white pellet of DNA. Supernatant was pipetted out of tubes and 100µl of 100% ethanol was added to each tube, which was then inverted several times to wash the DNA. Tubes were centrifuged again for 25 min. at 14,000g at room temperature and then the ethanol was aspirated as much as possible. Pellets were air-dried for 15 minutes and then 100µl of DNA rehydration solution (Promega) was added to each tube. Samples were left at room temperature for 1 hour and then stored in the refrigerator overnight.

PCR AMPLIFICATION

DNA samples were transferred from the refrigerator to a polystyrene ice bucket filled with crushed ice and samples were diluted (1:1) with DNA rehydration solution (Promega) before amplifying by PCR. PCR reaction mix was prepared in a sterile 1.5ml Eppendorf tube, which was pushed into a depression in the crushed ice (see Appendix B

for PCR reaction mix preparation details). For each PCR tube, 2.5µl of diluted DNA sample was added, followed by 0.2µl Taq polymerase and finally 20µl reaction mixture. PCR tubes were loaded into a Sprint PCR Thermocycler for DNA amplification.

ELECTROPHORESIS

Base-pair composition of the PCR reaction product was analyzed on a 2% agarose-gel by electrophoresis (LKB 2013 minophor submarine electrophoresis unit). Gel was viewed on a U-V trans-illumination table and bp number was estimated by comparing the bands produced by the PCR reaction product with those of a standard marker producing bands at precise 100 bp intervals. DNA was characterized by comparing bp number against that of a known DNA. DNA for mutant SOD1 displays a band at 230bp and DNA for method control interlukin-2 displays a band at 300bp. Based on these two bp numbers, the mice were genotyped as Tg or Wt. See appendix C for detailed electrophoresis procedural steps.

2.3. Perfusion-fixation for immunocytochemistry

All procedures conducted on living animals were performed by my project supervisor Tony Pullen under British Home Office approved license. The mice were anesthetized with an intraperitoneal injection of 0.75ml Domitor (1mg/ml medetomidine hydrochloride) and 0.75ml Ketaset (100mg/ml ketamine hydrochloride), which induces level 4 anesthesia. After loss of withdrawal, pinna and skin reflexes, the thorax was quickly opened and an intra-venous cannula was inserted into the left anterior aspect of the left ventricle. The right atrial appendage was snipped to allow blood leakage and perfusion was carried out with 50ml saline (20mM PBS, pH 7.3), followed by 50ml 4% paraformaldehyde (PFA) in 20mM PBS, pH7.5, followed by 50ml 4% PFA in 20mM PBS, pH 7.3 containing 20% sucrose as a cryoprotectant. The spinal cord was removed,

notched along its length to facilitate fixative absorption and submersed in 4% PFA in 20mM PBS, pH 7.3 containing 20% sucrose in a closed container. After ~1 hour, fixative was tipped out of container holding spinal cord and replaced with saline containing 30% sucrose. When spinal cord was no longer floating (~1 hour later), it was removed and frozen.

2.4. Freezing of tissue

Liquid nitrogen was collected (250-500ml) with a dewar flask and 50ml isopentane (GPR Rectapur) was poured into a 100ml plastic tripour beaker, which was then immersed into the dewar flask immediately above the liquid nitrogen surface in order to cool. Sections of cord (~4-5mm long) were placed on a 1.5cm^2 piece of thin cork surrounded on 4 sides with silver foil, using an orange cap hypodermic needle as a handle and a support for the cord. Specimens were immersed in the cooled isopentane for ~5 seconds and then removed and mounted with 30% Arabic gum mountant (Sigma) and re-immersed in the isopentane for ~10-15 seconds until completely frozen. Once completely frozen, specimen was wrapped in aluminium foil and placed in the freezer at -42°C.

2.5. Immunocytochemistry

Sections of 10-15μm thickness were cut on a cryostat (Bright OTF5000) set at -22°C, mounted on gelatin-chrome alum coated slides and allowed to air dry for approximately one hour. Sections were then rinsed in 20mM phosphate buffered saline (PBS), pH 7.3, containing 0.02M glycine (see Appendix D for buffer details) in order to remove any fixatives. Non-specific antigens were blocked with buffer applied to sections for 30-45 minutes with longer application times for thicker sections. Sections were washed with three changes of buffer, five minutes per change, and then incubated overnight at 4°C in

primary antibody against VAMP2, M-2, SP or VAChT diluted in buffer (see Table 2 for antibody details). Preliminary experiments involved all four antibodies, however, due to the inconsistent staining of anti-VAMP2 and M-2 antibodies, further experiments focused on SP and VAChT. After incubation in primary antibody, sections were washed with 5 changes of buffer, 5 min per change, and then incubated in biotinylated link antibody (Vector) diluted in buffer for 4 hours at room temperature. Sections were then washed with 4 changes of PBS-glycine buffer, 5 min per change, and then incubated overnight at 4°C in horseradish peroxidase (HRP)-labeled secondary antibody, streptavidin (Vector), diluted in buffer. The following day, sections were washed in stock 20mM PBS, pH 7.3 four times, 5 min per change. Secondary antibody was detected by developing sections in 1.3mM DAB-0.02% hydrogen peroxide mixture for 4 minutes. Longer developing times were slightly more effective for anti-M-2 and VAMP2 antibodies but staining was frequently difficult to visualize. After developing, sections were washed with 3 changes of PBS and mounted in Aquamount and coverslip. Sites of dark brown colouration were interpreted as sites of primary antibody immunoreactivity and synaptic synapses contacting MNs appeared as brown circles with a darker shade than surrounding staining.

Antibody	Species	Dilution	Source	Corresponding link antibody
VAChT*	Goat polyclonal	1:250	Chemicon	Rabbit anti-goat IgG (Vector)
Synaptophysin	Mouse monoclonal	1:200	Sigma	Goat anti-mouse IgG (Vector)
VAMP-2*	Rabbit polyclonal	1:200†	Chemicon	Goat anti-rabbit IgG (Vector)
M-2*	Rabbit polyclonal	1:200†	Chemicon	Goat anti-rabbit IgG (Vector)

Table 2. Primary antibodies used. *VAChT, vesicular acetylcholine transporter; VAMP-2, vesicle associated membrane protein-2; M-2, muscarinic acetylcholine receptor-2.
†Dilutions for VAMP-2 and M-2 produced inconsistent results.

2.6. Data collection & analysis

MNs that were analyzed were selected from the ventral horn of lumbar spinal cord. Images of MNs were obtained using a light microscope 100X oil magnification lens and a digital camera (Nikon COOLPIX 995) set at a constant magnification for all images.

Photoshop ver.5.0 was used to convert images to a black and white format and adjust the brightness and contrast in order to maximize visualization of synapses. Perimeter and cross-sectional area of MNs were calculated using the computer program SigmaScan and numbers of synapses were counted manually. All measurements generated by SigmaScan were converted to micrometer units based on the number of pixels per micrometer, which was calculated with the use of a stage micrometer. Synapse width was measured in millimeters from a printed black and white image generated in Photoshop ver.5.0 and then converted to micrometers.

2.7. Statistics

Results are expressed as mean ± standard deviation (SD). Statistical analyses were performed using two-tailed t-tests with two samples, assuming unequal variances, in order to compare data values between and within Wt and Tg groups. Histogram analysis of CSA data was used to compare the distribution profiles of groups with significantly different mean values. All statistical analyses were performed using computerized software (Excel 2003, Microsoft Office, USA) and the null hypothesis was rejected at the 0.05 level.

3. Results

3.1. General appearance and cross-sectional area of MNs evaluated

In both Wt and Tg mice from the 9-11 week age group, MNs from the ventral horn appeared intact and relatively large, with clearly delineated nuclei and cell membranes. Across all age groups, nuclei were not always visible and occasionally there was slight freezing damage, which appeared as random perforations throughout the cell. It was difficult to perceive differences in neuronal integrity between Wt and Tg mice in the 13

week age group. However, in clinically affected Tg animals, it was possible to visualize many damaged MNs with substantial vacuolation of the somata and nucleus, as well as erosion of the cell membrane. MNs from Wt animals remained relatively intact across all age groups.

Cross-sectional area (CSA) was calculated for each ventral horn MN analyzed from lumbar cord tissue sections stained for SP and VAChT (complete list of measurements in Appendix E). The CSA of SP-stained MNs (CSA-SP) in Tg mice from the pre-clinical age range ($369\mu m^2 \pm 174\mu m^2$, n=39) was similar to those of age-matched Wt mice ($363\mu m^2 \pm 152\mu m^2$, n=108, Fig. 1a). At 13 weeks, CSA-SP in Tg mice ($261\mu m^2 \pm 113\mu m^2$, n=78) was considerably smaller than those in age-matched Wt mice ($354\mu m^2 \pm 164\mu m^2$, n=65, p<0.001, Fig. 1a). Similarly, CSA-SP in Tg mice at 16-20 weeks ($246\mu m^2 \pm 110\mu m^2$, n=44) was somewhat smaller than that in age-matched Wt mice ($322\mu m^2 \pm 135\mu m^2$, n=58, p<0.01, Fig. 1a). The CSA of VAChT-stained MNs (CSA-VAChT) in Tg mice was similar to that in age-matched Wt mice within the 9-11 week and 16-20 week age ranges (Fig. 1b). There was, however, a significant difference between CSA-VAChT in Tg mice at 13 weeks ($277.4 \pm 109.0\mu m^2$, n=48) and CSA-VAChT in age-matched Wt mice ($395.2 \pm 170.4\mu m^2$, n=38, p<0.001, Fig. 1b). Histogram analysis of CSA-VAChT in Wt mice at 13 weeks revealed an abnormal distribution with few values near the mean and several high peaks lying far outside the center of the distribution (histogram not shown).

3.2. SP-immunostaining: synapse frequency

MNs immunostained for SP are depicted in Fig. 2 (Wt mice) and Fig. 3 (Tg mice), for all age ranges evaluated. In both Wt and Tg mice, across all ages, immunostaining for SP

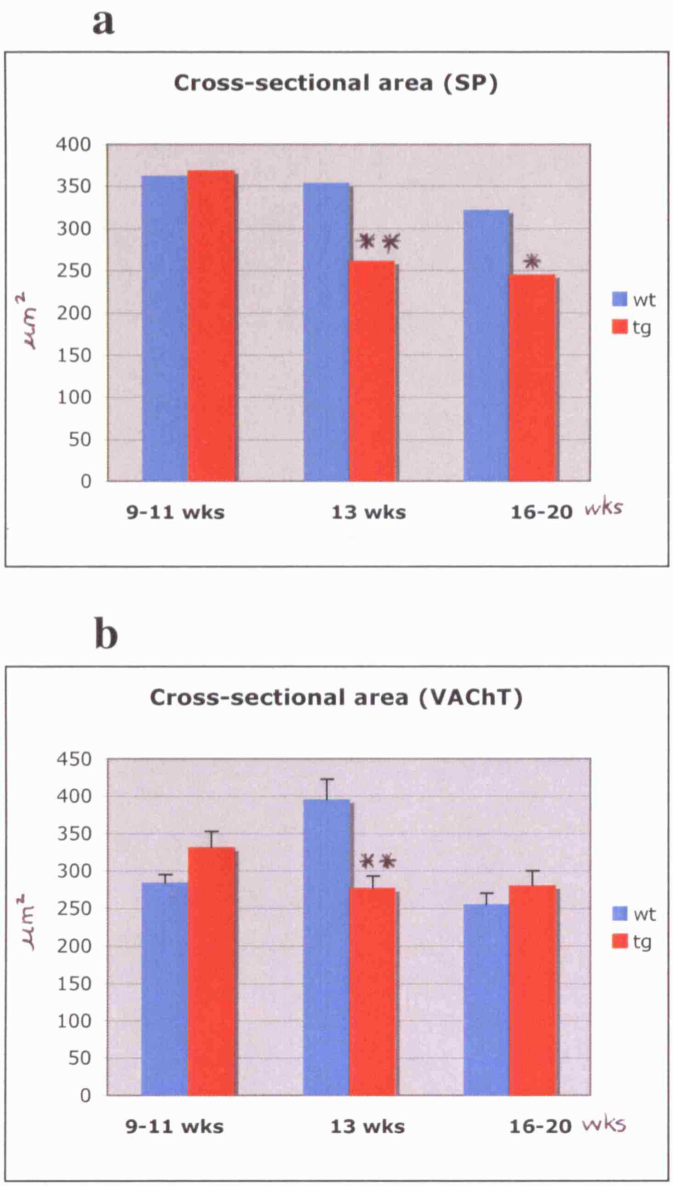

Figure 1. (A) Cross-sectional area (μm^2) of SP-stained MNs in Tg and Wt mice. Measurements show similar CSAs in Tg and Wt mice at 9-11 weeks, significantly smaller CSAs in Tg mice at 13 weeks (261.4 ± 113.2μm^2, n=78) compared to age-matched Wt mice (354.0 ± 163.9μm^2, n=65, $^{**}p<0.001$) and significantly smaller CSAs in Tg mice at 16-20 weeks (245.5 ± 109.9μm^2, n=44) compared to age-matched Wt mice (322.1 ± 135.3μm^2, n=58, $^{*}p<0.01$). (B) Cross-sectional area (μm^2) of VAChT-stained MNs in Tg and Wt mice. Measurements show similar CSAs in Tg and Wt mice at 9-11 weeks, significantly smaller CSAs in Tg mice at 13 weeks (277.4 ± 109.9μm^2, n=48) compared to age-matched Wt mice (395.2 ± 170.4μm^2, n=38, $^{**}p<0.001$) and similar CSAs in Tg and Wt mice at 16-20 weeks.

resulted in darkly coloured synapses contacting the membrane and faint staining within the cell body, while the nucleus generally remained light in appearance. Synapse frequency was calculated as the number of synapses immunoreactive for SP per 100μm of neuronal membrane. Pre-clinical Tg mice exhibited similar numbers of SP-IR

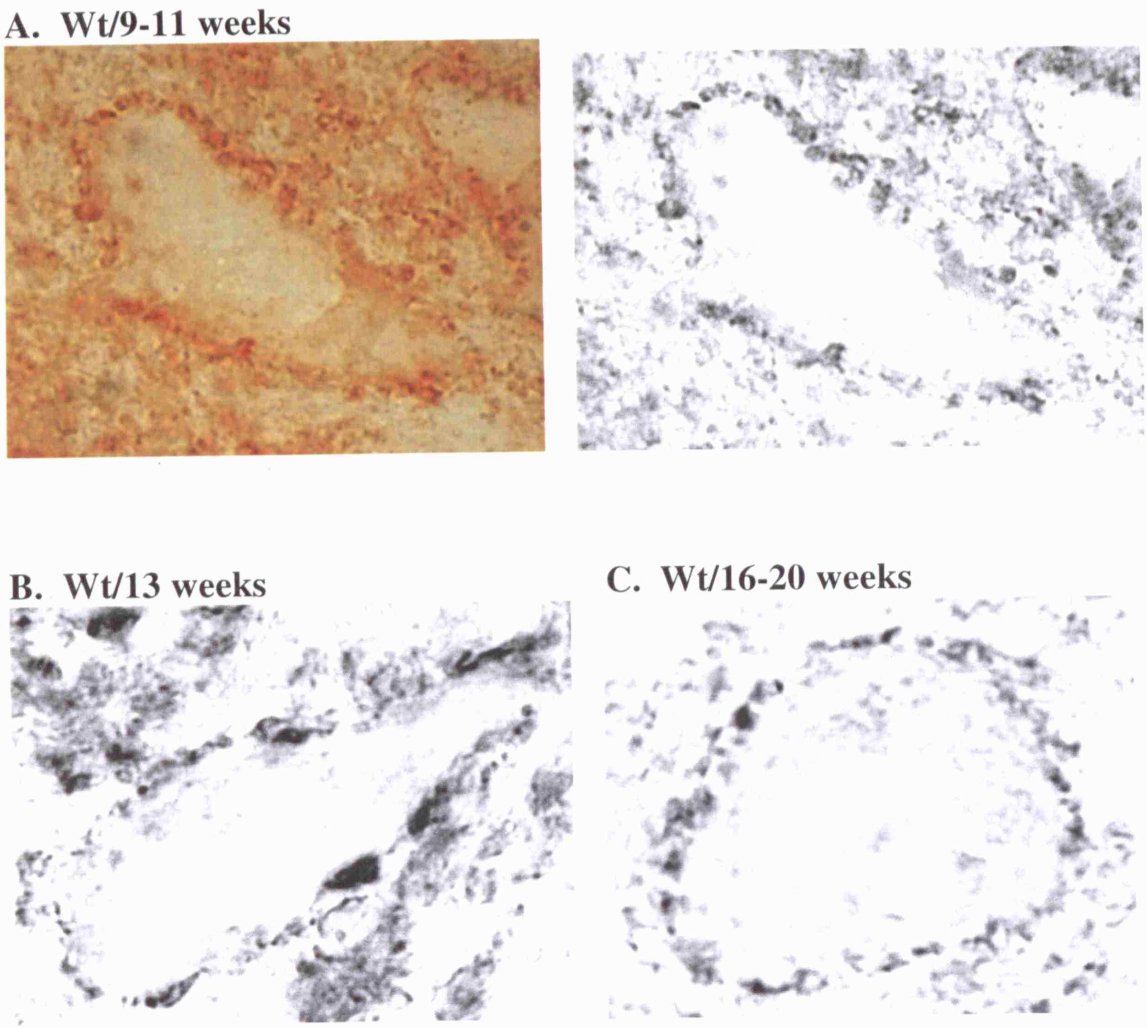

Figure 2. Immunocytochemistry using antibody against **SP** in lumbar cord ventral horns of Wt mice at 9-11 weeks (A), 13 weeks (B) and 16-20 weeks (C). (A) Original digital photograph and its corresponding black and white version that was used for analysis.

synapses in the ventral horn (39.2 ± 7.74, n=39) compared to age-matched Wt mice (37.1 ± 7.13, n=108, Fig. 4a,b). There was a progressive decrease in SP-IR synapses contacting MNs in Tg mice throughout the course of disease. Transgenic mice at 13 weeks of age exhibited significantly fewer stained synapses (27.4 ± 10.6, n=78) compared to Wt mice in the same age group (34.2 ± 10.6, n=65, p<0.001, Fig. 4a,b). By end-stage disease Tg mice showed a 65% overall reduction in synapses contacting ventral horn MNs that resulted in a synapse frequency of 13.6 ± 5.02 (n=44), which was 46% of the frequency in

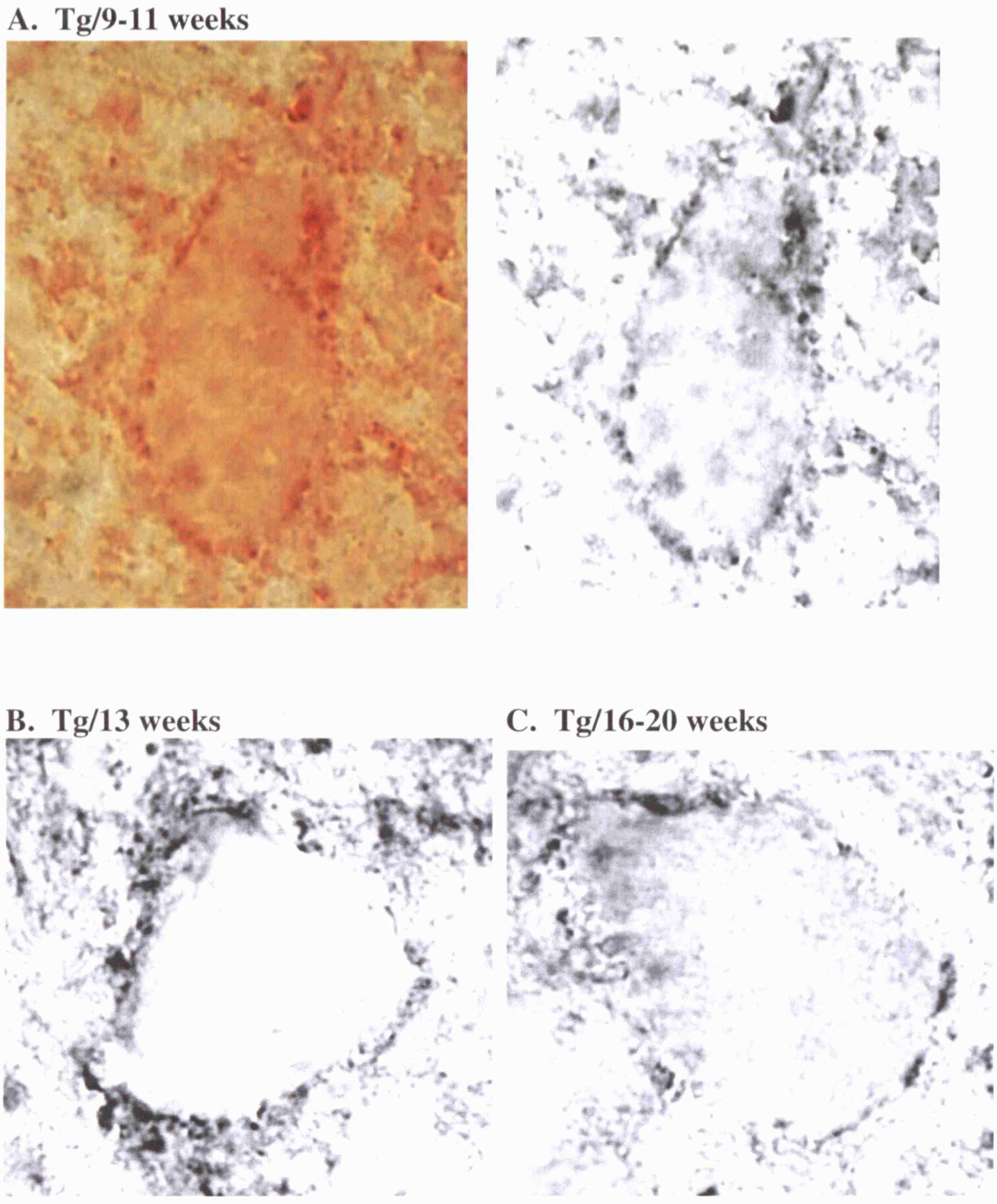

Figure 3. Immunocytochemistry using antibody against **SP** in lumbar cord ventral horns of Tg mice at 9-11 weeks (A), 13 weeks (B) and 16-20 weeks (C). (A) Original digital photograph and its corresponding black and white version that was used for analysis.

age-matched Wt mice (29.6 ± 9.08, n=58, p<0.001, Fig. 4a,b). Collected data related to synapse frequency in SP-stained tissue from Wt and Tg mice, across all age ranges evaluated, are summarized in Table 3.

3.3. VAChT-immunostaining: synapse frequency

MNs immunostained for VAChT are depicted in Fig. 5 (Wt mice) and Fig. 6 (Tg mice), for all age ranges evaluated. VAChT-stained MNs exhibited highly stained synaptic synapses apposing the neuronal membrane and moderate staining of the cell body, with the nucleus mostly remaining light in appearance. Frequently the cell bodies were also heavily stained and the synapses appeared only slightly darker. Synapse frequency was calculated as the number of synapses immunoreactive for VAChT per 100μm of neuronal membrane. Within the pre-clinical age range, Tg mice were found to have a somewhat lower synapse frequency (12.2 ± 5.20, n=35) compared to age-matched Wt mice (15.9 ± 5.87, n=92, p<0.01, Fig. 7a,b). At 13 weeks, Tg mice continued to have significantly lower VAChT-IR synapse frequency (14.6 ± 6.82, n=48) compared to age-matched Wt mice (19.6 ± 7.43, n=38, p<0.01, Fig. 7a,b), although the difference was much less than that seen with SP staining in the same age group. Also contrary to results found with SP staining, VAChT-IR synapse frequency in clinically affected Tg mice (10.9 ± 5.35, n=48) was relatively similar to that in age-matched Wt mice (12.5 ± 4.91, n=45, Fig. 7a,b). Collected data related to synapse frequency in VAChT-stained tissue from Wt and Tg mice, across all age ranges evaluated, are summarized in Table 3.

3.4. VAChT-immunostaining: synapse width

Estimations of VAChT-IR synapse width in MNs from Wt and Tg mice, for pre-clinical and clinical age ranges, are summarized in Table 4. Within the 9-11 week age

range, the width of VAChT-IR synaptic synapses in Tg mice (3.62μm ± 0.703μm, mean ± SD, n=212) was slightly smaller compared to the Wt group (3.82μm ± 0.772μm, p<0.01, Fig. 8). By end-stage disease, synaptic terminal sizes in Tg mice (6.90μm ± 1.68μm, n=314) had increased by a factor of 1.91 and were significantly larger than synapse sizes in age-matched Wt mice (5.12μm ± 1.52μm, n=231, p<0.001, Fig. 8).

SYNAPSE FREQUENCY	Wild-type SP	Transgenic SP	Wild-type VAChT	Transgenic VAChT
9-11 weeks	Mean f=1.24 SD=0.238 N=108 Minimum=0.789 Maximum=2.117	Mean f=1.31 SD=0.259 N=39 Minimum=0.594 Maximum=1.90	Mean f=0.532 SD=0.196 N=92 Minimum=0.225 Maximum=1.28	Mean f=0.407 SD=0.174 N=35 Minimum=0.188 Maximum=1.01
13 weeks	Mean f=1.14 SD=0.354 N=65 Minimum=0.471 Maximum=1.88	Mean f=0.914 SD=0.355 N=78 Minimum=0.204 Maximum=1.78	Mean f=0.655 SD=0.248 N=38 Minimum=0.142 Maximum=1.05	Mean f=0.486 SD=0.228 N=48 Minimum=0.143 Maximum=1.04
16-20 weeks	Mean f=0.989 SD=0.303 N=58 Minimum=0.369 Maximum=2.00	Mean f=0.452 SD=0.168 N=44 Minimum=0.124 Maximum=0.830	Mean f=0.418 SD=0.164 N=45 Minimum=0.134 Maximum=0.874	Mean f=0.363 SD=0.178 N=48 Minimum=0.155 Maximum=0.822

Table 3. Synapse frequency (f), measured as the number of stained synaptic synapses per 100μm neuronal membrane, from Wt and Tg mice stained for SP and VAChT.

SYNAPSE WIDTH (μM)	Wild-type	Transgenic
9-11 weeks	Mean=3.82 SD=0.772 N=331 Minimum=1.71 Maximum=6.83	Mean=3.62 SD=0.703 N=212 Minimum=1.75 Maximum=5.97
16-20 weeks	Mean=5.12 SD=1.52 N=231 Minimum=2.56 Maximum=10.2	Mean=6.90 SD=1.68 N=314 Minimum=3.41 Maximum=11.9

Table 4. Estimated VAChT-IR synaptic terminal width (μm), standard deviation (SD), and sample size (N) in Wt and Tg mice.

a

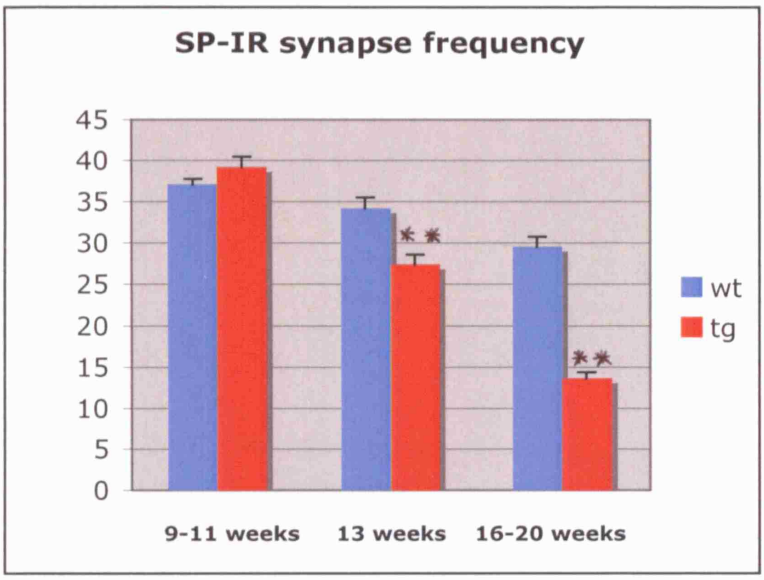

b

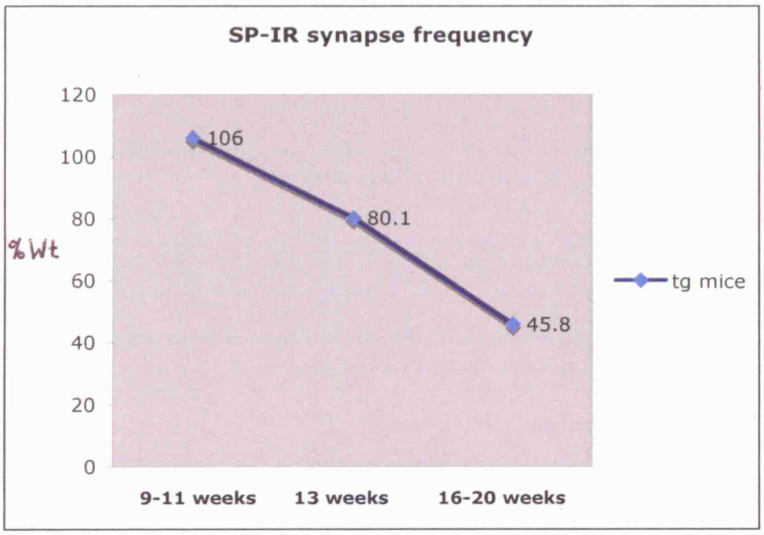

Figure 4. (A) Mean SP-IR synapse frequency (# of synapses per 100μm neuronal membrane). Immunocytochemistry shows there is no significant difference between Tg mice at 9-11 weeks (1.31 ± 0.259, n=39) compared to age-matched Wt mice (1.24 ± 0.238, n=108). There are significantly fewer SP-IR synapses in Tg mice at 13 weeks (0.914 ± 0.355, n=78) compared to age-matched Wt mice (1.14 ± 0.354, n=65, ** p<0.001) and significantly fewer SP-IR synapses in Tg mice at 16-20 weeks (0.452 ± 0.168, n=44) compared to age-matched Wt mice (0.989 ± 0.303, n=58, ** p<0.001). (B) Tg SP-IR synapse frequency shown as a percentage of mean Wt frequency.

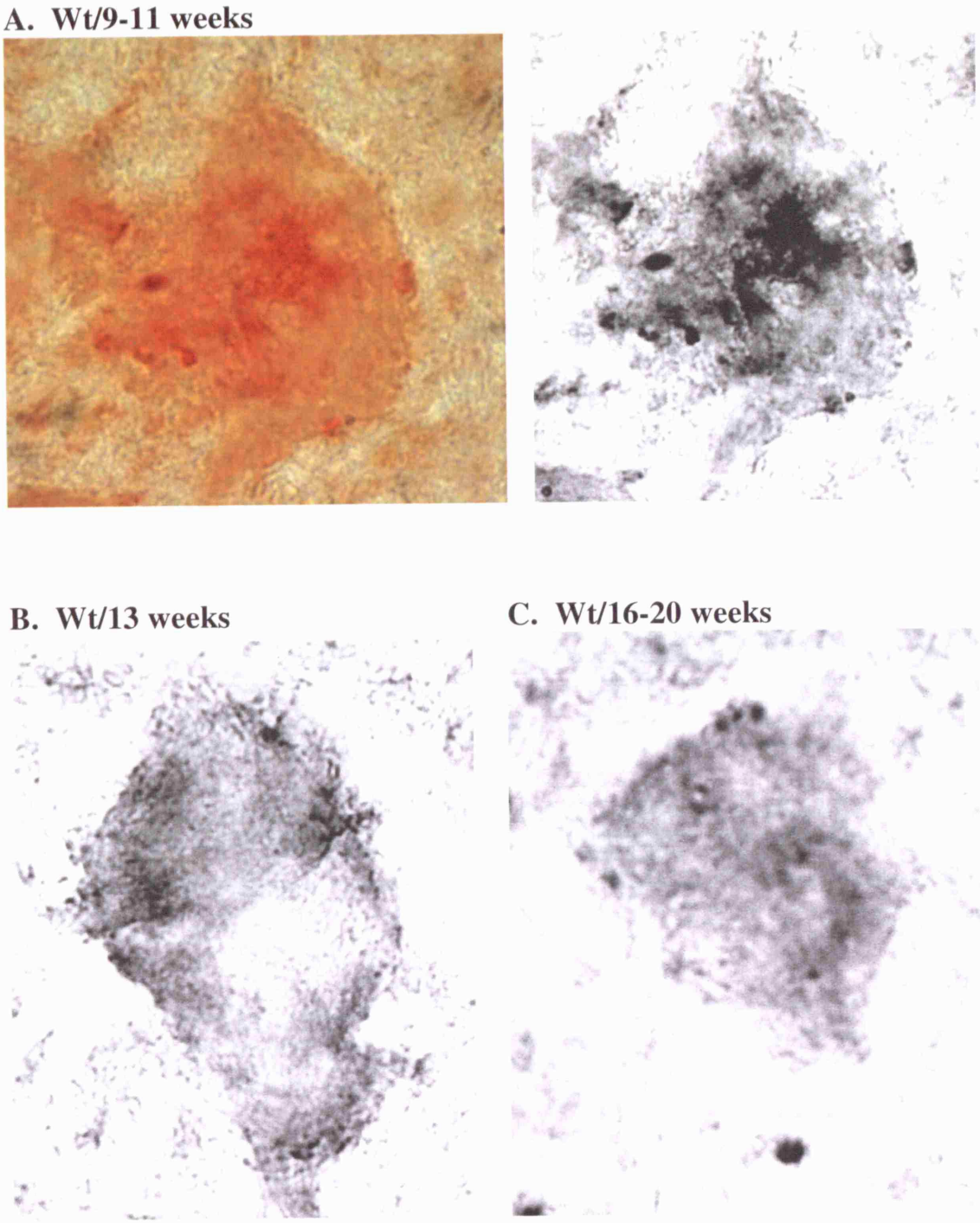

Figure 5. Immunocytochemistry using antibody against **VAChT** in lumbar cord ventral horns of Wt mice at 9-11 weeks (A), 13 weeks (B) and 16-20 weeks (C). (A) Original digital photograph and its corresponding black and white version that was used for analysis.

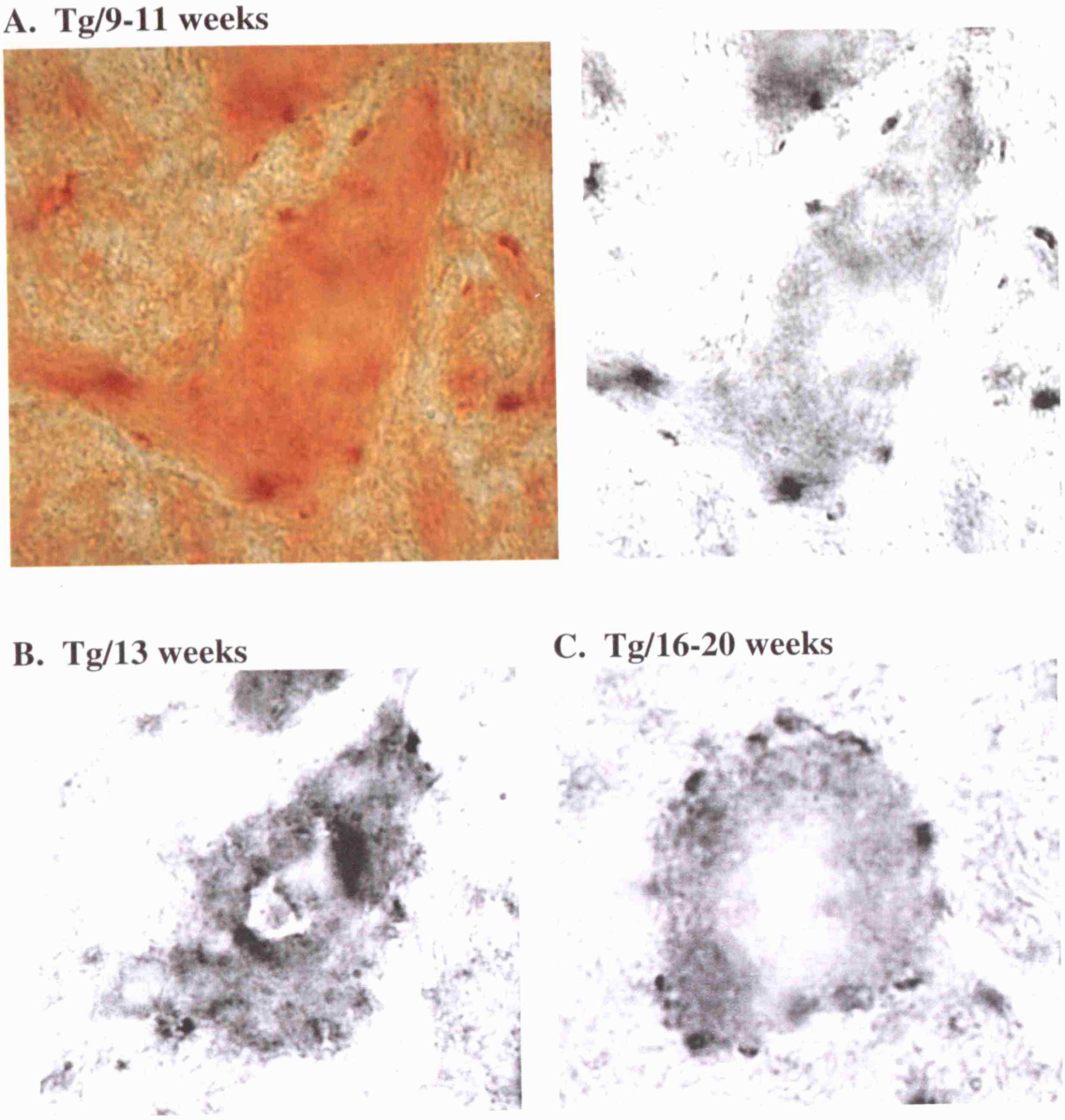

Figure 6. Immunocytochemistry using antibody against **VAChT** in lumbar cord ventral horns of Tg mice at 9-11 weeks (A), 13 weeks (B) and 16-20 weeks (C). (A) Original digital photograph and its corresponding black and white version that was used for analysis.

4. Discussion

CSA was measured in order to strengthen the assumption that each group of MNs examined across all time points evaluated were chosen from the same population of ventral horn neurons and would therefore have a similar range of CSA. With SP immunostaining, Wt mice displayed consistent mean CSA across all ages, which supported the assumption that all MNs examined were chosen from the same population.

Unexpectedly, there was a significant decrease in mean CSA seen in Tg mice at 13 weeks and 16-20 weeks, which was likely a result of the small and unequal sample size of the MN groups examined. VAChT staining revealed consistent mean CSA in Tg mice across all age ranges, however, there was an unexpected increase in mean CSA in Wt mice at 13 weeks. It seems most probable that the anomalies in mean CSA in both SP-stained Tg mice and VAChT-stained Wt mice were due to small and unequal sample size as apposed to age-dependent changes in neuronal CSA. There was a wide range of CSA values within all groups, which increased the likelihood of acquiring significantly different means. With larger sample sizes, it would be beneficial to determine whether significant changes occurred in neuronal size and then factor in the size change when calculating synapse frequency.

SP immunostaining revealed that Tg mice underwent a progressive loss of synapses contacting ventral horn MNs, which was significant by 13 weeks and resulted in approximately 50% synapse loss by end-stage disease. These findings are consistent with previous literature indicating a widespread decrease of SP-IR synapses in ALS patients and G93A SOD1 mice (Ikemoto & Hirano, 1996; Zang et al., 2005) and confirm the effectiveness of general immunostaining procedures used in the study. While the initial drop in VAChT-IR synapse frequency at 13 weeks in Tg mice likely signifies an early stage of MN degeneration involving loss of neuronal communication, VAChT-IR synapse frequencies in Wt and Tg mice were not significantly different in the 16-20 week age range, which starkly contrasts SP staining results. The pattern of VAChT-IR synapse frequency in Tg mice consisting of a dip at 13 weeks followed by a rise at the late clinical stage supports earlier EM results obtained from experiments with the same mouse model of fALS (Pullen & Athanasiou, 2007). Increased VAChT-IR synapse frequency also supports the hypothesis

that C-synapses are resistant to degeneration and provide a compensatory means of communication for MNs in the ventral horn.

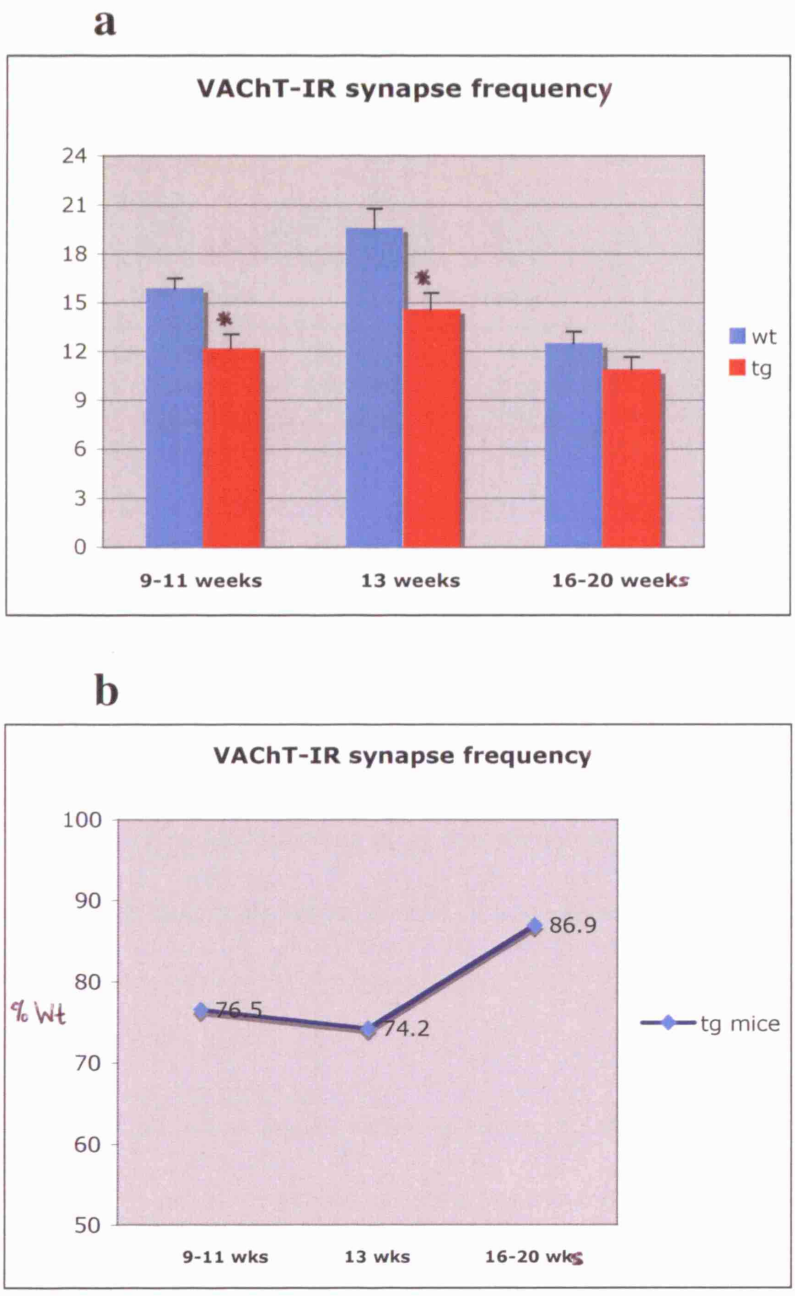

Figure 7. (a) Mean VAChT-IR synapse frequency (# of synapses per 100µm neuronal membrane). Immunocytochemistry shows significantly fewer VAChT-IR synapses in Tg mice at 9-11 weeks (0.407 ± 0.174, n=35) compared to age-matched Wt mice (0.532 ± 0.196, n=92, * p<0.01) and significantly fewer VAChT-IR synapses in Tg mice at 13 weeks (0.486 ± 0.228, n=48) compared to age-matched Wt mice (0.655 ± 0.248, n=38, * p<0.01). There is no significant difference between Tg mice at 16-20 weeks (0.363 ± 0.228, n=48) compared to age-matched Wt mice (0.418 ± 0.164, n=45). (b) Tg VAChT-IR synapse frequency shown as a percentage of mean Wt frequency.

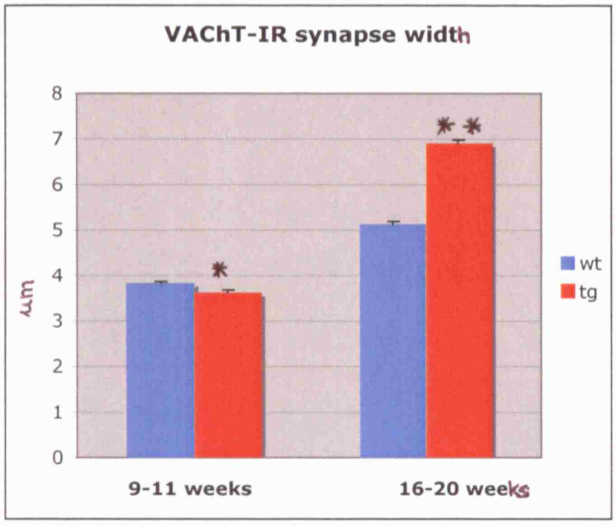

Figure 8. Mean estimated width (µm) of VAChT-IR synapses. Measurements show somewhat smaller synapse width in Tg mice at 9-11 weeks (3.62 ± 0.703µm, *n*=212) compared to age-matched Wt mice (3.82 ± 0.772µm, *n*=331, * $p<0.01$). Synapse width in Tg mice at 16-20 weeks (6.90 ± 1.68µm, *n*=314) is substantially larger compared to age-matched Wt mice (5.12 ± 1.52µm, *n*=231, ** $p<0.001$).

In regard to the size of VAChT-IR synapses, it is worth noting the increase in synapse width seen in Tg mice. While mean synapse width in Wt mice did increase somewhat by 16-20 weeks, this was only by a factor of 1.3, whereas the mean synapse width in Tg mice increased by a factor of 1.9 over the same period. The finding of increased synapse size in clinically affected mice complements previous EM findings in ALS patients and Tg mice indicating an expansion of post-synaptic territory of C-synapses on surviving MNs during the clinical stage of ALS (Pullen et al., 1992; Pullen & Athanasiou, 2007).

The fact that VAChT-IR synapses were not subject to the same reduction as SP-IR synapses indicates that this group of synapses could possess a quality that allows them to elude the general synaptic loss seen in ALS. Size, origin, morphology and plasticity may all be factors that confer a degree of resistance to C-synapses under neurodegenerative conditions. The relatively large size of C-synapses under normal conditions might be associated with a large energy supply that allows the synapse to survive a neurotoxic environment that is destructive to smaller synapses. It is also possible that the putative

interneuronal origin of C-synapses is less susceptible to disease than the dorsal root and descending fiber origins of other synapse types in the spinal cord. In addition, the rER subtending C-synaptic cisterns may provide essential proteins to MNs that are beneficial under disease conditions. These qualities in conjunction with the plastic extension of pre- and post-synaptic territory as well as an increased frequency of C-synapses may contribute to C-synapse disease resistance. Furthermore, the cholinergic and potentially muscarinic nature of C-synapses facilitates modulation of MN excitability (Miles et al., 2007), which could potentially counteract disease-mediated loss of excitability.

The most prominent methodological weaknesses of the study originated from small sample sizes and limitations involving VAChT-immunostaining. Unfortunately, sample size was affected by time restrictions, which prevented larger samples of neurons from being evaluated, and by financial resources, which precluded the use of large amounts of antibody and additional mice. The unpredictable nature of the antibody against VAChT caused frequent heavy staining within neuronal cell bodies in addition to synapses, which interfered with the accurate quantification of VAChT-IR synapses. Additional time for optimizing staining techniques might greatly reduce the difficulties in identifying VAChT-IR synapses. As with any study examining C-synapses, using immunocytochemistry to identify C-type synapses isn't entirely conclusive without complementary EM confirmation of the synapse type. It is very likely that the cholinergic synapses contacting large α MNs in the ventral horn are C-synapses but it is possible that some cholinergic synapses are not C-type based on previous work identifying C-synapses in rodent spinal cord (Nagy et al., 1993; Li et al., 1995).

Despite the limitations of this study, the results are interesting because they confirm previous EM findings indicating an increase in size and number of C-syanpses in progressed stages of ALS. In the future, it may be beneficial to examine the correlation

between the presence of C-synapses and GAP-43 accumulation on spinal MNs in animal models of ALS. Since GAP-43 has been shown to accumulate in ventral horn MNs in patients with ALS (Parhad et al., 1992; Ikemoto et al., 1999), it would be interesting to determine whether this accumulation shows a relationship with increased numbers of C-synapses. If GAP-43 accumulation is paralleled by an increase in C-synapses, then GAP-43-induced afferent nerve sprouting may be the source of increased C-synapses and a mechanism of protection against neuronal degeneration. Alternatively, it is possible that an increase in GAP-43 is related to MN axons sprouting out to denervated muscle fibers, which could depend on the additional synaptic information reaching spinal MNs via an increased number of C-synapses. On the other hand, increased synaptic communication via C-synapses may work to offset a neurodegenerative effect of GAP-43-induced collateral sprouting. In light of previous findings of intense GAP-43 immunoreactivity in Onuf's nucleus, which is preserved in ALS (Swash & Schwartz, 1995; Brook et al., 1998), it seems likely that GAP-43 accumulation plays a protective role in ALS.

From a therapeutic standpoint, since C-synapses are found upregulated on MNs that have managed to survive until late stages of ALS, it could be beneficial to understand the molecular mechanisms behind C-synapse disease resistance and the effect of this resistance on the electrical potential of late-surviving MNs. There may be a substantial excitatory impact on MNs with upregulated C-syanpses, which would likely be enhanced by the apparent increase in synapse width and postsynaptic territory. Furthermore, increased excitation of MNs during mid-to-late stages of ALS may work to counteract the loss of motor function. The data reported here suggest that C-synapses are able to resist degradation of synaptic input to spinal MNs by increasing in size and number, which points toward a potential defense mechanism against neurodegeneration and impaired motor function in the present model of human fALS.

References

Al-Chalabi, A. (2006) Motor neuron disease. *ACNR* 6:7-8.

Azzouz, M., Leclerc, N., Gurney, M., Warter, J.M., Poindron, P. and Borg, J. (1997) Progressive motro neuron impairment in an animal model of familial amyotrophic lateral sclerosis. *Muscle & Nerve* 20:45-51.

Bodian, D. (1966) Synaptic types on spinal motoneurons. An electron microscopic study. *Bull Hopkins Hosp* 119:16-45.

Boillee, S., Yamanaka, K., Lobsiger, C.S., Copeland, N.G., Jenkins, N.A., Kassiotis, G., Kollias, G., Cleveland, D.W. (2006) Onset and progression in inherited ALS determined by motor neurons and microglia. *Science* 312:1389-1392.

Boone, T.B. and Aldes, L.D. (1984) Synaptology of the hypoglossal nucleus in the rat. *Exp Brain Res* 57:22-32.

Borchelt, D.R., Lee, M.K., Slunt, H.S., Guarnieri, M., Xu, Z.S., Wong, P.C., Brown, Jr, R.H., Price, D.L., Sisodia, S.S. and Cleveland, D.W. (1994) Superoxide dismutase 1 with mutations linked to familial amyotrophic lateral sclerosis possesses significant activity. *PNAS USA* 91:8292-8296.

Brook, G.A., Schmitt, A.B., Nacimiento, W., Weis, J., Schröder, J.M., Noth, J. (1998) Distribution of B-50(GAP-43) mRNA and protein in the normal adult human spinal cord. *Acta neuropathologica* 95: 378-386.

Bruijn, L.I., Becher, M.W., Lee, M.K., Anderson, K.L., Jenkins, N.A., Copeland, N.G., Sisodia, S.S., Rothstein, J.D., Borchelt, D.R., Price, D.L. and Cleveland, D.W. (1997a) ALS-linked SOD1 mutant G85R mediates damage to astrocytes and promotes rapidly progressive disease with SOD1-containing inclusions. *Neuron* 18:327-338.

Bruijn, L.I., Beal, M.F., Becher, M.W., Schulz, J.B., Wong, P.C., Price, D.L. and Cleveland, D.W. (1997b) Elevated free nitrotyrosine levels, but not protein-bound nitrotyrosine or hydroxyl radicals, throughout amyotrophic lateral sclerosis (ALS)-like disease implicate tyrosine nitration as an aberrant in vivo property of one familial ALS-linked superoxide dismutase-1 mutant. *PNAS USA* 94:7606-7611.

Chen, Y.Z., Bennett, C.L., Huynh, H.M., Blair, I.P., Puls, I., Irobi, J., Dierick, I., Abel, A., Kennerson, M.L., Rabin, B.A., Nicholson, G.A., Auer-Grumbach, M., Wagner, K., De Jonghe, P., Griffin, J.W., Fischbeck, K.H., Timmerman, V., Cornblath, D.R. and Chance, P.F. (2004) DNA/RNA helicase gene mutations in a form of juvenile amyotrophic lateral sclerosis (ALS4). *Am J Hum Genet* 74:1128–1135.

Chio, A., Benzi, G., Dossena, M., Mutani, R. and Mora, G. (2005) Severely increased risk of amyotrophic lateral sclerosis among Italian professional football players. *Brain* 128:472-476.

Chiu, A.Y., Zhai, P., Dal Canto, M.C., Peters, T.M., Kwon, Y.W., Prattis, S.M. and Gurney, M.E. (1995) Age-dependent penetrance of disease in a transgenic mouse model of familial amyotrophic lateral sclerosis. *Mol Cell Neurosci.* 6:349-362.

Connaughton, M., Priestley, J.V., Sofroniew, M.V., Eckenstein, F. and Cuello, A.C. (1986) Inputs to motoneurons in the hypoglossal nucleus of the rat: light and electron microscopic immunocytochemistry for choline acetyltransferase, substance P and enkephalins using monoclonal antibodies. *Neurosci* 17:205-224.

Conradi, S. (1969a) Ultrastructure and distributions of neuronal and glial elements on the motoneuron surface in the lumbosacral spinal cord of the adult cat. *Acta Physiol Scand*, Suppl, 332:5-48.

Conradi, S. (1969b) Ultrastructure and distributions of neuronal and glial elements on the Surface of the proximal part of a motoneuron dendrite, as analyzed by serial sections. *Acta Physiol Scand*, Suppl, 332:49-64.

Dal Canto, M.C. and Gurney, M.E. (1995) Neuropathology changes in two lines of mice carrying a transgene for mutant human Cu,Zn SOD, and in mice overexpressing wild type human SOD: A model of familial amyotrophic lateral sclerosis (FALS). *Brain Res* 676:25-40.

Dal Canto, M.C. and Gurney, M.E. (1997) A low expresser line of transgenic mice carrying

a mutant human Cu,Zn superoxide dismutase (SOD-1) gene develops pathological changes that most closely resemble those in human amyotrophic lateral sclerosis. *Acta Neuropathol* 93:537-550.

Deng, H.X., Hentati, A., Tainer, J.A., Iqbal, Z., Cayabyab, A., Hung, W.Y., Getzoff, E.D., Hu, P., Herzfeldt, B., Roos, R.P., Warner, C., Deng, G., Soriano, E., Smyth, C., Parge, H.E., Ahmed, A., Roses, A.D., Hallewell, R.A., Pericak-Vance, M.A. and Siddiqueet, T. (1993) Amyotrophic lateral sclerosis and structural defects in Cu,Zn superoxide dismutase. *Science* 261:1047-1051.

Elliott, J.L. (1999) Experimental models of amyotrophic lateral sclerosis. *Neurobiol Dis* 6:310-320.

Feeney, S.J., McKelvie, P.A., Austin, L., Jean-Francois, B., Kapsa, R., Tombs, S.M. and Byrne, E. (2001) Presymptomatic motor neuron loss and reactive astrocytosis in the SOD1 mouse model of amyotrophic lateral sclerosis. *Muscle & Nerve* 24:1510-1519.

Fischer, L.R., Culver, D.G., Tennant, P., Davis, A.A., Wang, M., Castellano-Sanchez, A., Khan, J., Polak, M.A. and Glass, J.D. (2004) Amyotrophic lateral sclerosis is a distal axonopathy: evidence in mice and man. *Exp Neurol* 185:232-240.

Fujii, J., Myint, T., Seo, H.G., Kayanoki, Y., Ikeda, Y. and Taniguchi, N. (1995) Characterization of wild-type and amyotrophic lateral sclerosis-related mutant Cu,Zn-superoxide dismutases overproduced in baculovirus-infected insect cells. *J Neurochem* 64:1456-1461.

Gilmor, M.L., Nash, N.R., Roghani, A., Edwards, R.H., Yi, H., Hersch, S.M. and Levey, A.I. (1996) Expression of the putative vesicular acetylcholine transporter in rat brain and localization in cholinergic synaptic vesicles. *J Neurosci* 16:2179-2190.

Gurney, M.E., Pu, H., Chiu, A.Y., Dal Canto, M.C., Polchow, C.Y., Alexander, D.D., Caliendo, J., Hentati, A., Kwon, Y.W., Deng, H.X., Chen, W., Zhai, P., Sufit, R.L. and Siddique, T. (1994) Motor neuron degeneration in mice that express a human Cu,Zn superoxide dismutase mutation. *Science* 264:1772-1775.

Gurney, M.E. (1997) Transgenic animal models of familial amyotrophic lateral

sclerosis. *J. Neurol* 244 Suppl 2:S15-S20.

Halliwell, B., Gutteridge, J.M.C. and Cross, C.E. (1992) Free radicals, antioxidants, and human disease: Where are we now? *J Lab Clin Med* 119:598-620.

Halliwell, B. (1994) Free radicals, antioxidants, and human disease: curiosity, cause, or consequence? *Lancet* 344:721-724.

Hamson, D.K., Hu, J.H., Krieger, C. and Watson, N.V. (2002) Lumbar motoneuron fate in a mouse model of amyotrophic lateral sclerosis. *NeuroReport* 13:2291-2294.

Hellstrom, J., Arvidsson, U., Elde, R. Cullheim, S. and Meister, B. (1999) Differential expression of nerve terminal protein isoforms in VAChT-containing varicosities of the spinal cord ventral horn. *J Comp Neurol* 411:578-590.

Hellstrom, J., Oliveira, A.L.R., Meister, B. and Cullheim, S. (2003) Large cholinergic nerve terminals on subsets of motoneurons and their relation to muscarinic receptor type 2. *J Comp Neurol* 460:476-486.

Horner, R.D., Kamins, K.G., Feussner, J.R., Grambow, S.C., Hoff-Lindquist, J., Harati, Y., Mitsumoto, H., Pascuzzi, R., Spencer, P.S., Tim, R., Howard, D., Smith, T.C., Ryan, M.A.K., Coffman, C.J., Kasarskis, E.J. (2003) Occurrence of amyotrophic lateral sclerosis among Gulf War veterans. *Neurology* 61:742-749.

Ichikawa, T., Ajikia, K., Matsuurab, J. and Misawa, H. (1997) Localization of two cholinergic markers, choline acetyltransferase and vesicular acetylcholine transporter in the central nervous system of the rat: in situ hybridization histochemistry and immunohistochemistry. *J Chem Neuroanat* 13:23-39.

Ikemoto, A. and Hirano, A. (1996) Comparative immunohistochemical study on synaptophysin expression in the anterior horn of post-poliomyelitis and sporadic amyotrophic lateral sclerosis. *Acta Neuropathol* 92:473-478.

Ikemoto, A., Hirano, A. and Akiguchi, I. (1999) Increased expression of growth-associated protein 43 on the surface of the anterior horn cells in amyotrophic lateral sclerosis. *Acta Neuropathol* 98:367-373.

Ischiropoulos, H. and Al-Mehdi, A.B. (1995) Peroxynitrite-mediated oxidative protein

modification. *FEBS Lett* 364:279-282.

Jaarsma, D., Guchelaar, H.J., Haasdijk, E., de Jong, V. and Holstege, J.C. (1998) The antioxidant N-acetylcysteine does not delay disease onset and death in a transgenic mouse model of amyotrophic lateral sclerosis. *Ann Neurol* 44:293.

Kennel, P.F., Finiels, F., Revah, F. and Mallet, J. (1996) Neuromuscular function impairment is not caused by motor neurone loss in FALS mice: an electromyographic study. *NeuroReport* 7:1427-1431.

Kiernan, J.A. and Hudson, A.J. (1993) Changes in shapes of surviving motor neurons in amyotrophic lateral sclerosis. *Brain* 116:203-215.

Knyihar-Csillik, E., Csillik, B. and Oestreicher, A.B. (1992) Light and electron microscope localization of B-50 (GAP43) in the rat spinal cord during transganglionic degenerative atrophy and regeneration. *J Neurosci Res* 32:93-109.

Kong, J. and Xu, Z. (1998) Massive mitochondria degeneration in motor neurons triggers the onset of amyotrophic lateral sclerosis in mice expressing a mutant SOD1. *J Neurosci* 18: 3241-3250.

Kostic, V., Gurney, M.E., Deng, H.X., Siddique, T., Epstein, C.J. and Przedborski, S. (1997) Midbrain dopaminergic neuronal degeneration in a transgenic mouse model of familial amyotrophic lateral sclerosis. *Ann Neurol* 41:497-504.

Kunst, C.B. (2004) Complex genetics of amyotrophic lateral sclerosis. *Am J Hum Genet* 75:933–947.

Kusaka, H. and Hirano, A. (1999) Cytopathology of the motor neuron. In: Younger, D.S. (ed.) *Motor Disorders*, Philadelphia: Lippincott Williams & Wilkins, pp. 93-101.

Li, W., Ochalski, P.A.Y., Brimijoin, S., Jordan, L.M. and Nagy, J.I. (1995) C-terminals on motoneurons: electron microscope localization of cholinergic markers in adult rats and antibody-induced depletion in neonates. *Neurosci* 65:879-891.

McLaughlin, B.J. (1972) The fine structure of neurons and synapses in the motor nuclei of the cat spinal cord. *J Comp Neurol* 144:429-460.

Miles, G.B., Hartley, R., Todd, A.J. and Brownstone, R.M. (2007) Spinal cholinergic interneurons

regulate the excitability of motoneurons during locomotion. *PNAS USA* 104:2448-2453.

Mohajeri, M.H., Figlewicz, D.A. and Bohn, M.C. (1998) Selective loss of α motoneurons innervating the medial gastrocnemius muscle in a mouse model of amyotrophic lateral sclerosis. *Exp Neurol* 150:329-336.

Morrison, B.M., Gordon, J.W., Ripps, M.E. and Morrison, J.H. (1996) Quantitative immunocytochemical analysis of the spinal cord in G86R superoxide dismutase transgenic mice: neurochemical correlates of selective vulnerability. *J Comp Neurol* 373:619-631.

Morrison, B.M., Janssen, W.G., Gordon, J.W. and Morrison, J.H. (1998a) Time course of neuropathology in the spinal cord of G86R superoxide dismutase transgenic mice. *J Comp Neurol* 391:64-77.

Morrison, B.M., Morrison, J.H. and Gordon, J.W. (1998b) Superoxide dismutase and neurofilament transgenic models of amyotrophic lateral sclerosis. *J Expt Zool* 282:32-47.

Morrison, B.M. and Morrison, J.H. (1999) Amyotrophic lateral sclerosis associated with mutations in superoxide dismutase: a putative mechanism of degeneration. *Brain Res Rev* 29:121-135.

Mulder, D.W. (1982) in Rowland, L.P. (ed.) *Human Motor Neuron Diseases*, New York: Raven, pp. 15-22.

Mulder, D.W., Kurland, L.T., Offord, K.P. and Beard, C.M. (1986) Familial adult motor neuron disease: amyotrophic lateral sclerosis. *Neurology* 36:511-517.

Nagy, J.I., Yamamoto, T. and Jordan, L.M. (1993) Evidence for the cholinergic nature of C-terminals associated with subsurface cisterns in α-motoneurons of rat. *Synapse* 15:17-32.

Navone, F., Jahn, R., Di Gioia, G., Stukenbrok, H., Greengard, P. and De Camilli, P. (1986) Protein p38: an integral protein specific for small vesicles of neurons and neuroendocrine cells. *J Cell Biol* 103:2511-2527.

Neve, R.L., Perrone-Bizzozero, N.I., Finklestein, S., Zwiers, H., Bird, E., Kurnit, D.M. and

Benowitz, L.I. (1987) The neuronal growth-associated protein GAP-43 (B-50,F1): neuronal specificity, developmental regulation and regional distribution of the human and rat mRNAs. *Mol Brain Res* 2:177-183.

Nguyen, M.D., Boudreau, M., Kriz, J., Couillard-Després, S., Kaplan, D.R. and Julien, J.P. (2003) Cell cycle regulators in the neuronal death pathway of amyotrophic lateral sclerosis caused by mutant superoxide dismutase 1. *J Neurosci* 23:2131-2140.

Nishimura, A.L., Mitne-Neto, M., Silva, H.C.A., Richieri-Costa, A., Middleton, S., Cascio, D., Kok, F., Oliveira, J.R.M., Gillingwater, T., Webb, J., Skehel, P. and Zatz, M. (2004) A mutation in the vesicle-trafficking protein VAPB causes late-onset spinal muscular atrophy and amyotrophic lateral sclerosis. *Am J Hum Genet* 75:822–831.

Olanow, C.W. and Arendash, G.W. (1994) Metals and free radicals in neurodegeneration. *Curr Opin Neurol* 7:548-558.

Oyanagi, K., Makifuchi, T. and Ikuta, F. (1983) A topographical and quantitative study of neurons in human spinal gray matter, with special reference to their changes in amyotrophic lateral sclerosis. *Biomed Res* 4:211-224.

Pardo, C.A., Xu, Z., Borchelt, D.R., Price, D.L., Sisodia, S.S. and Cleveland, D.W. (1995) Superoxide dismutase is an abundant component in cell bodies, dendrites, and axons of motor neurons and in a subset of other neurons. *PNAS USA* 92:954-958.

Parhad, I.M., Oishi, R. and Clark, A.W. (1992) GAP-43 gene expression is increased in anterior horn cells of amyotrophic lateral sclerosis. *Ann Neurol* 31:593-597.

Pullen, A.H. and Sears, T.A. (1978) Modification of 'C' synapses following partial central deafferentation of thoracic motoneurones. *Brain Res* 145:141-146.

Pullen, A.H., Martin, J.E. and Swash, M. (1992) Ultrastructure of pre-synaptic input to motor neurons in Onuf's nucleus: controls and motor neuron disease. *Neuropathol Appl Neurobiol* 18:213-231.

Pullen, A.H. and Martin, J.E. (1995) Ultrastructural abnormalities with inclusions in Onuf's nucleus in motor neuron disease (amyotrophic lateral sclerosis). *Neuropathol Appl Neurobiol* 21:327-340.

Pullen, A.H. and Athanasiou, D. (2007) Selective compensatory increase in presynaptic territory on lumbar motorneurones by a propriospinal synapse in a mouse model of MND/ALS. *ALS* 8 Suppl 1:157-158.

Reaume, A.G., Elliott, J.L., Hoffman, E.K., Kowall, N.W., Ferrante, R.J., Siwek, D.R., Wilcox, H.M., Flood, D.G., Beal, M.F., Brown Jr., R.H., Scott R.W. and Snider W.D. (1996) Motor neurons in Cu/Zn superoxide dismutase-deficient mice develop normally but exhibit enhanced cell death after axonal injury. *Nature Genet* 13:43-47.

Ripps, M.E., Huntley, G.W., Hof, P.R., Morrison, J.H. and Gordon, J.W. (1995) Transgenic mice expressing an altered murine superoxide dismutase gene provide an animal model of amyotrophic lateral sclerosis. *PNAS USA* 92:689-693.

Rosen, D.R., Siddique, T., Patterson, D., Figlewicz, D.A., Sapp, P., Hentati, A., Donaldson, D., Goto, J., O'Regan, J.P., Deng, H.X., Rahmani, Z., Krizus, A., McKenna-Yasek, D., Cayabyab, A., Gaston, S.M., Berger, R., Tanzi, R.E., Halperin, J.J., Herzfeldt, B., Van den Bergh, R., Hung, W.Y., Bird, T., Deng, G., Mulder, D.W., Smyth, C., Laing, N.G., Soriano, E., Pericak-Vance, M.A., Haines, J., Rouleau, G.A., Gusella, J.S., Horvitz, H.R. and Brown Jr., R.H. (1993) Mutations in Cu/Zn superoxide dismutase gene are associated with familial amyotrophic lateral sclerosis. *Nature* 362:59-62.

Sasaki, S. and Iwata, M. (1999) Ultrastructural change of synapses of Betz cells in patients with amyotrophic lateral sclerosis. *Neurosci. Letters* 268:29-32.

Schaefer, A.M., Sanes, J.R. and Lichtman, J.W. (2005) A compensatory subpopulation of motor neurons in a mouse model of amyotrophic lateral sclerosis. *J Comp Neurol* 490:209-219.

Schäfer, M.K., Eiden, L.E. and Weihe, E. (1998) Cholinergic neurons and terminal fields revealed by immunohistochemistry for the vesicular acetylcholine transporter. I. Central nervous system. *Neuroscience* 84:331-359.

Schutz, B. (2005) Imbalanced excitatory to inhibitory synaptic input precedes motor neuron degeneration in an animal model of amyotrophic lateral sclerosis. *Neurobiol Dis* 20:131-140.

Shibata, N., Nagai, R., Miyata, S., Jono, T., Horiuchi, S., Hirano, A., Kato, S., Sasaki, S., Asayama, K. and Kobayashi, M. (2000a) Nonoxidative protein glycation is implicated in familial amyotrophic lateral sclerosis with superoxide dismutase-1 mutation. *Acta Neuropathol* 100:275-284.

Shibata, N., Hirano, A., Yamamoto, T., Kato Y. and Kobayashi, M. (2000b) Superoxide dismutase-1 mutation-related neurotoxicity in familial amyotrophic lateral sclerosis. *ALS* 1:143-161.

Shibata, N. (2001) Transgenic mouse model for familial amyotrophic lateral sclerosis with superoxide dismutase-1 mutation. *Neuropathology* 21:82-92.

Siddique, T., Pericak-Vance, M.A., Brooks, B.R., Roos , R.P., Hung, W.Y., Antel, J.P., Munsat, T.L., Phillips, K., Warner, K., Speer, M., Bias, W.B., Siddique, N.A. and Roses, A.D. (1989) Linkage analysis in familial amyotrophic lateral sclerosis. *Neurology* 39:919-925.

Skene, J.H.P. (1989) Axonal growth-associated proteins. *Ann Rev Neurosci* 12:127-156.

Stephens, B., Guiloff, R.J., Navarrete, R., Newman, P., Nikhar, N. and Lewis, P. (2006) Widespread loss of neuronal populations in the spinal ventral horn in sporadic motor neuron disease. A morphometric study. *J Neurol Sci* 244:41-58.

Swash, M. and Schwartz, M.S. (1995) Motor Neuron Disease: The Clinical Syndrome. In: Leigh, P.N. and Swash, M. (ed.) *Motor Neuron Disease, Biology and Management* London: Springer-Verlag.

Tandan, R. and Bradley, W.G. (1985a) Amyotrophic lateral sclerosis: part 1. Clinical features, pathology, and ethical issues in management. *Ann Neurol* 18:271-280.

Tandan, R. and Bradley, W.G. (1985b) Amyotrophic lateral sclerosis: part 2. Etiopathogenesis. *Ann Neurol* 18:419-431.

Tu, P.-H., Raju, P., Robinson, K.A., Gurney, M.E., Trojanowski, J.Q. and Lee, V.M. (1996) Transgenic mice carrying a human mutant superoxide dismutase transgene develop neuronal cytoskeletal pathology resembling human amyotrophic lateral sclerosis lesions. *PNAS USA* 93:3155-3160.

Tysnes, O. (2004) Epidemiology and Management of ALS. *ACNR* 4:8-9.

Ueki, A., Namba, Y., Otsuka, M., Okuno, M., Nishimura, M., Oda, M. and Ikeda, K. (1993) GAP-43 immunoreactivity is detected in the nerve terminals of patients with amyotrophic lateral sclerosis. *Ann Neurol* 33:226-227.

Urushitani, M., Ezzi, S.A. and Julien, J. (2007) Therapeutic effects of immunization with mutant superoxide dismutase in mice models of amyotrophic lateral sclerosis. *PNAS USA* 104:2495-2500.

Verhaagen, J., Oestreicher, A.B., Edwards, P.M., Veldman, H., Jennekens, F.G.I. and Gispen, W.H. (1988) Light and electron-microscopical study of phosphoprotein B-50 following denervation and reinnervation of the rat soleus muscle. *J Neurosci* 8:1759-1766.

Warita, H., Itoyama, Y. and Abe, K. (1999) Selective impairment of fast anterograde axonal transport in the peripheral nerves of asymptomatic transgenic mice with a G93A mutant SOD1 gene. *Brain Res* 819:120-131.

Williamson, T.L. and Cleveland, D.W. (1999) Slowing of axonal transport is a very early event in the toxicity of ALS-linked SOD1 mutants to motor neurons. *Nature Neuroscience* 2:50-56.

Wohlfart, G. (1957) Collateral regeneration from residual motor nerve fibers in amyotrophic lateral sclerosis. *Neurology* 7:124-134.

Wong, P.C., Pardo, C.A., Borchelt, D.R., Lee, M.K., Copeland, N.G., Jenkins, N.A., Sisodia, S.S., Cleveland, D.W. and Price, D.L. (1995) An Adverse Property of a Familial ALS-Linked SOD1 Mutation Causes Motor Neuron Disease Characterized by Vacuolar Degeneration of Mitochondria. *Neuron* 14:1105-1116.

Yang, Y., Hentati, A., Deng, H.X., Dabbagh, O., Sasaki, T., Hirano, M., Hung, W.Y., Ouahchi, K., Yan, J., Azim, A.C., Cole, N., Gascon, G., Yagmour, A., Ben-Hamida, M., Pericak-Vance, M., Hentati, F. and Siddique, T. (2001) The gene encoding alsin, a protein with three guanine-nucleotide exchange factor domains, is mutated in a form of recessive amyotrophic lateral sclerosis. *Nat Genet* 29:160–165.

Yu, B.P. (1994) Cellular defenses against damage from reactive oxygen species. *Physiol Rev*

74:139-162.

Zang, D.W. and Cheema, S.S. (2002) Degeneration of corticospinal and bulbospinal systems in the superoxide dismutase $1^{G93A\ G1H}$ transgenic mouse model of familial amyotrophic lateral sclerosis. *Neurosci Lett* 332:99-102.

Zang, D.W., Lopes, E.C. and Cheema, S.S. (2005) Loss of synaptophysin-positive synapses on lumar motor neurons innervating the medial gastrocnemius muscle of the $SOD1^{G93A\ G1H}$ transgenic mouse model of ALS. *J Neurosci Res* 79:694-699.

Appendix A:

Mouse ID	Genotype	Age (weeks)	Sex	Weight (g)	Markings **
AT3	Wt	9	f	17.8	brown/REM
AT2	Tg	9	f	18.3	brown/NEM
AU7	Tg	10	f	16.9	white/NEM
AU9	Wt	10	f	18.7	brown/NEM
BH3	Tg	10	m	23.4	brown/REM
AS5	Wt	11	f	20.4	white/NEM
AS6	Tg	11	f	18.1	brown/NEM
BH2	Wt	11	m	25.1	brown/REM
BO10	Wt	11	f	16.1	brown/NEM
BP11	Wt	11	f	20.5	white/REM
AU3	Tg	13	m	25.2	brown/LEM
AU2	Wt	13	m	22.5	brown/REM
AS2	Wt	13	m	36.0	beige/REM
AS4	Tg	13	m	28.2	brown/NEM
BI4	Tg	13	m	34.2	white/RLEM
BH4	Wt	13	m	31.8	black/REM
JD1	Wt	16	f	24.7	white/REM
JD2	Wt	16	f	21.08	brown/REM
AR5	Wt	16	m	30.0	beige/NEM
AX2	Tg	16	f	16.0	brown/REM
JD4	Tg	17	m	20.4	brown/REM
JD3	Tg	18	m	20.7	brown/LEM
BF1	Tg	18	m	24.4	brown/NEM
AY4	Wt	19	m	28.3	brown/LREM
BE2	Wt	20	m	32.9	brown/NEM
BB1	Tg	20	m	27.7	brown/NEM

Table 5. List of mice used for experiments. * f=female, m=male, ** REM=right ear mark, LEM=left ear mark, NEM=no ear mark, LREM=both left and right ear mark.

Appendix B:

PCR reaction mix preparation steps

1. Each of the following reagents added to a 1.5ml Eppendorf tube, pushed into a depression in crushed ice, in the following order:
   - DEPC-treated, autoclaved water (14µl)
   - Qiagen* solution 'Q' (4µl)
   - PCR Buffer (10X) (2µl)
   - $MgCl_2$ (1µl)
   - dNTP mix (0.2µl)
   - Primer 1-forward reaction, mutant SOD1 (0.25µl)
   - Primer 2-reverse reaction, mutant SOD1 (0.25µl)
   - Primer 3-forward reaction, method control DNA: IL-2 (0.25µl)
   - Primer 4-reverse reaction, method control DNA: IL-2 (0.25µl)
   - Taq polymerase-**added after step 3** (0.2µl)

2. Vortex reagents for 5 seconds.

3. Add 2.5µl diluted DNA sample to each PCR tube.

4. Add Taq polymerase.

5. Using separate pipette tips for each PCR tube, add 20µl reaction mixture per tube.

* Qiagen 'Core' PCR kit contains: 'Q' solution, 10X TRIS-HCL PCR buffer, $MgCl_2$, dNTP, Taq. Components include: TRIS-HCL buffer, KCl, NH_4SO_4, $MgCl_2$.

Appendix C:

Electrophoresis Reagents

1. DEPC-treated, autoclaved distilled water; 500ml distilled water + 0.5ml diethyl pyrocarbonate
2. Sample buffer (Invitrogen 'Blue juice'); 10mM TRIS-HCI, pH 7.5, 10mM EDTA, 0.3% bromophenol blue
3. 10X TBE Buffer; To prepare 10X concentration, dissolve 10.8g TRIS base and 5.5g Boric acid in 80ml DEPC-treated, autoclaved distilled water. Add 4ml of 0.5M EDTA, pH 8.0 (= 0.76g/4ml). Mixture may need warming to 37°C to assist dissolving. EDTA may precipitate out when cold. Stored at room temperature.
4. Running buffer; 1X dilution = 20ml 10X TBE added to 200ml DEPC treated water. Add 20µl 5mg/ml ethidium bromide.
5. 2% Low melting point agarose in TBE; Prepare 2% solution in 1X TBE buffer as follows:
    1. Dilute 2.5ml 10X TBE buffer to 22.5ml with DEPC-treated water.
    2. Heat 1X TBE on hot-plate/stirrer to 70-80°C, covering with glass funnel to prevent evaporation.
    3. Slowly add 0.5g agarose powder, maintaining temperature and stirring continuously. Agarose will form gelatinous mass, which can be broken up with sterile glass rod. Mass will slowly dissolve if stirring is maintained.
    4. When fully dissolved, add 2.5µl of 5mg/ml ethidium bromide.
    5. Allow to cool to 55°C before casting gel.
6. Ethidium bromide (5mg/ml solution in DEPC-treated water); Weigh out 5ml ethidium bromide and dissolve in 1ml treated water.

Electrophoresis Method

1. Place gel casting tray on level surface with end-stop plates and comb in appropriate slots. All parts clean and dry.
2. Prepare 2% agarose gel as described above.
3. Gently pour gel onto running plate and allow gel to cool and polymerise. Cover tray with cling-film to prevent dust contamination.
4. After ~1 hour, gel should set. Remove comb by lifting at a slight angle (pulling vertically creates vacuum in wells and may lift entire gel out of casting tray).
5. Place gel and casting tray in electrophoresis unit, and fill unit with running buffer containing 0.5µg/ml ethidium bromide to a level that just covers the gel by about 1mm (~150ml buffer).
6. Load DNA samples mixed with sample buffer with a micropipette (~1518µl/well), filling one well with an appropriate DNA marker and if possible another well with a positive control.
7. Carefully place lid on unit so the cathode is at the end nearest the sample wells. Push connectors down as far as possible.
8. With unit turned OFF, connect power cables to power unit, switch on unit and set voltage/time settings.
9. Surround entire unit with crushed ice to cool the unit.
10. Monitor gel as it runs, using blue dye in the sample as a guide.
11. On completion, switch off power unit and disconnect leads from power unit before opening the lid. Gel is now ready for viewing on UV trans-illumination table.

Appendix D:

Reagents

The following solutions were used to prepare buffers used in the experiments.

Solution A: 200mM sodium dihydrogen phosphate dihydrate ($NaH_2PO_4.2H_2O$)
In a 500ml sterile plastic culture flask, dissolved 15.6g of $NaH_2PO_4.2H_2O$ in total volume of 500ml deionised water.

Solution B: 200mM disodium hydrogen phosphate.12 H_2O ($Na_2HPO_4.12H_2O$)
In a 500ml sterile plastic culture flask, dissolved 14.15g of $Na_2HPO_4.12H_2O$ in total volume of 500ml deionised water.

Solution C: Stock 20mM phosphate buffered saline (PBS), pH 7.3
In a 100ml glass measuring cylinder, added 19ml Solution A to 81ml Solution B. Poured into 1000ml beaker and diluted to 900ml with deionised water. Added 8.67g NaCl, checked pH and adjusted if necessary with 1N NaOH or 1N HCl. Final volume adjusted to 1000ml with deionised water. Stored in fridge at 4°C. This solution was used as the base component for the following series of buffers.

Buffer (i): 20mM PBS buffer, pH 7.3, containing 0.02M glycine
In 500ml solution C, dissolved 0.75g glycine. Used this to make buffers (ii-vii).

Buffer (ii): 20mM PBS-glycine buffer pH 7.3 containing 3% bovine serum albumin (BSA) +3% normal goat serum (NGS). Used as blocking buffer for slides with antibody against SP, M-2 and VAMP-2.

Buffer (iii): 20mM PBS-glycine buffer pH 7.3 containing 3% BSA + 3% normal rabbit serum (NRS). Used as blocking buffer for slides with antibody against VAChT.

Buffer (iv): 20mM PBS-glycine buffer pH 7.3 containing 0.1% BSA + 0.1% NGS. Used as secondary antibody dilution buffer and washing buffer for slides with antibody against SP, M-2 and VAMP-2.

Buffer (v): 20mM PBS-glycine buffer pH 7.3 containing 0.1% BSA. Used as secondary antibody dilution buffer and washing buffer for slides with antibody against VAChT.

Buffer (vi): 20mM PBS-glycine buffer pH 7.3 containing 0.5% BSA + 0.5% NGS. Used as primary and link antibody dilution buffer for slides with antibody against SP, M-2 and VAMP-2.

Buffer (vii): 20mM PBS-glycine buffer pH 7.3 containing 0.5% BSA + 0.5% NRS. Used as primary and link antibody dilution buffer for slides with antibody against anti-VAChT.

Appendix E:

CROSS-SECTIONAL AREA (μm^2)	Wild-type SP	Transgenic SP	Wild-type VAChT	Transgenic VAChT
9-11 weeks	Mean=362.7 SD=151.5 *N*=108 Minimum=99.09 Maximum=817.3	Mean=368.9 SD=174.4 *N*=39 Minimum=126.4 Maximum=901.6	Mean=284.2 SD=104.9 *N*=92 Minimum=110.0 Maximum=583.2	Mean=331.5 SD=123.8 *N*=35 Minimum=111.0 Maximum=582.2
13 weeks	Mean=354.0 SD=163.9 *N*=65 Minimum=126.7 Maximum=899.9	Mean=261.4 SD=113.2 *N*=78 Minimum=59.82 Maximum=573.3	Mean=395.2 SD=170.4 *N*=38 Minimum=95.48 Maximum=683.3	Mean=277.4 SD=109.9 *N*=48 Minimum=97.52 Maximum=555.2
16-20 weeks	Mean=322.1 SD=135.3 *N*=58 Minimum=106 Maximum=670.9	Mean=245.5 SD=109.9 *N*=44 Minimum=60.08 Maximum=594.3	Mean=255.3 SD=99.77 *N*=45 Minimum=98.05 Maximum=542.5	Mean=280.7 SD=133.9 *N*=48 Minimum=71.53 Maximum=634.2

Table 6. Cross-sectional area measurements in square microns (μm^2) from wt and tg mice stained for SP and VAChT.